Icarus 228 (2014) 13–26

Contents lists available at ScienceDirect

Icarus

journal homepage: www.elsevier.com/locate/icarus

Formation of brucite and cronstedtite-bearing mineral assemblages on Ceres

Mikhail Yu. Zolotov *

School of Earth and Space Exploration, Arizona State University, Tempe, AZ 85287-1404, USA

ARTICLE INFO

Article history:
Received 25 June 2013
Revised 10 September 2013
Accepted 23 September 2013
Available online 1 October 2013

Keywords:
Asteroid Ceres
Mineralogy
Asteroids, composition
Asteroids, surfaces
Cosmochemistry

ABSTRACT

Dwarf planet Ceres is the largest body in the main asteroid belt with a rocky surface and uncertain internal structure. Spectra of Ceres in near- and mid-infrared wavelengths are consistent with the occurrence of brucite, Mg-bearing carbonates, and an Fe-rich phyllosilicate cronstedtite. Spectra of 10 Hygiea and 324 Bamberga imply similar compositions. Here, we considered stabilities of these minerals to constrain their origin. Cronstedtite is most stable at the temperature of ~0 °C at moderately oxidizing aqueous conditions and at high water/rock ratios. Although cronstedtite could form on planetesimals, the apparent lack of serpentine may indicate its formation by Ceres' temporary surface solutions. Brucite forms at a low activity of dissolved SiO_2, at a low fugacity of CO_2, and at highly alkaline *pH*. Brucite and cronstedtite do not form together and may not form deep in the Ceres' interior. The absence of Mg serpentine from Ceres' surface materials and the unlikely occurrence of very olivine-rich rocks do not indicate a formation of brucite through serpentinization of such rocks. Brucite could form by transient near-surface fluids which do not equilibrate with silicates. Temporary fluids could deposit Mg carbonates before, after, or together with brucite at near-surface conditions that favor CO_2 degassing. Regardless of Ceres' internal structure, internal thermal and aqueous processes may not affect cold near-surface layers. Percolation of interior fluids is not consistent with the lack of detection of low-solubility salts. However, impacts of ice-rich targets during the Late Heavy Bombardment could account for transient aqueous environments and unusual surface mineralogies of Ceres, Hygiea, and Bamberga. Brucite and Mg carbonates could have formed through hydration and carbonation of MgO evaporated from silicates. Apparently abundant carbonates may indicate an ample impact oxidation of organic matter, and the occurrence of brucite with cronstedtite may reflect turbulent and disequilibrium environments. Clay-like homogeneous surface materials on Ceres could be gravitationally sorted deposits of impact clouds.

1. Introduction

Dwarf planet (1) Ceres is the largest and most massive body in the main asteroid belt (Table 1; McCord et al., 2011). The polar flattening determined with Hubble Space Telescope is consistent with a relaxed differentiated body with a rocky core and an icy mantle (Thomas et al., 2005; Castillo-Rogez and McCord, 2010), though such an internal structure awaits verification. Initially accreted rocks may not survive atop a water mantle because they would silk through the ice or an ocean (McCord and Sotin, 2005), and the origin of unique spectral characteristics of Ceres' rocky surface (Rivkin et al., 2011) remains to be understood in the framework of a differentiated structure. Ceres' dimensions determined with the Keck II telescope (Carry et al., 2008) do not exclude the undifferentiated or partially differentiated body without icy mantle (Zolotov, 2009). In the latter case, Ceres could consist of hydrated ice-poor rocks with ~10% porosity similar to compacted CI/CM carbonaceous chondrites. Circular albedo features (Li et al., 2006; Carry et al., 2008, 2012) may be indicative of impact craters, consistent with craters on other asteroids and cratering models for Ceres (de Elía and Di Sisto, 2011). Large craters may either reflect a mantle-free internal structure or signify an impact deposition of rocks atop an icy mantle, as we discuss below. These controversies could be resolved after the determination of Ceres' gravity moments together with surface topography and morphology with Dawn in 2015 (Russell et al., 2007). Additional constrains could be gained from composition of surface materials, if formation conditions of observed minerals and chemical patters are understood.

1.1. Observational data on surface composition

The current knowledge about Ceres' surface mineralogy is based on telescopic observations in the ultraviolet, visible, near-, and mid-infrared (IR) spectral ranges (Table 2; Rivkin et al., 2011). Ceres has the visual geometric albedo of ~0.09 with very minor

* Fax: +1 (480) 965 8102.
E-mail address: zolotov@asu.edu

0019-1035/$ - see front matter © 2013 Elsevier Inc. All rights reserved.
http://dx.doi.org/10.1016/j.icarus.2013.09.020

Table 1
Physical characteristics of asteroids with the 3.06 μm spectral feature.

	Diameter (km)[a]	Mass (kg)	Density (g/cm^3)
1 Ceres	945 ± 23	$9.44 \pm 0.06 \times 10^{20}$	2.13 ± 0.15
		$9.35 \pm 0.14 \times 10^{20}$[b]	2.11 ± 0.35[c]
10 Hygiea	422 ± 26	$8.63 \pm 0.52 \times 10^{19}$	2.19 ± 0.42
		$8.67 \pm 0.15 \times 10^{19}$[d]	2.08 ± 0.10[d]
324 Bamberga	235 ± 8	$1.03 \pm 0.10 \times 10^{19}$	1.52 ± 0.20

Notes: The data are mostly from Carry (2012).
[a] The volume-equivalent diameter.
[b] Kovačevič (2012).
[c] Based on the mass from Kovačevič (2012) and the diameter from Carry (2012).
[d] Baer et al. (2011).

(<6%) variations (Li et al., 2006; Carry et al., 2008, 2012). The centimeter-wave, millimeter-wave, and sub-millimeter observations indicate a low-density dry clay-like surface material with a low thermal inertia and high porosity (Webster et al., 1988; Mitchell et al., 1996; Chamberlain et al., 2009). Despite a similarity of Ceres' near-IR reflectance spectra with that of metamorphosed carbonaceous chondrites (Hiroi et al., 1995), there is no good meteoritic spectral analog for Ceres' materials (Rivkin et al., 2011). The broad absorption feature near 3 μm indicates a presence of hydrated and/or OH-bearing minerals (Lebofsky, 1978; Lebofsky et al., 1981; Feierberg et al., 1981). Ceres' near- and mid-IR spectra are consistent with the presence of Fe phyllosilicate cronstedtite (Rivkin et al., 2006; Milliken and Rivkin, 2009) (Tables 2 and 3). Although cronstedtite provides a better fit of mid-IR spectra than Mg-serpentine (Milliken and Rivkin, 2009), a dominance of cronstedtite among surface silicates needs confirmation. Magnetite could account for by a broad absorption at ~1.2 μm (Larson et al., 1979; Rivkin et al., 2011) and darken Ceres' spectra in a broad range of wavelengths (Milliken and Rivkin, 2009). However, the occurrence of magnetite is not very certain because other phases (e.g., sulfides, organic species) could be darkening agents. There are clear spectral features of Mg-bearing carbonates (Rivkin et al., 2006; Milliken and Rivkin, 2009; Rivkin and Volquardsen, 2010), which could be much more abundant than in carbonaceous chondrites (typically < 2–3 vol.%; Brearley and Jones, 1998). Although strong spectral features of suggested minerals apparently indicate their high abundances, exact volume fractions may not be evaluated from current data. The features may represent coatings rather than bulk mineral contents in surface materials. It follows that some surface minerals could be present but not seen in the reflection and emission spectra.

Table 2
Minerals suggested in Ceres' surface materials based on telescopic observations in the near- and mid-IR spectral ranges.

Mineral	References
Mg carbonates[a]	Rivkin et al. (2006), Milliken and Rivkin (2009) and Rivkin and Volquardsen (2010)
Brucite	Milliken and Rivkin (2009)
Cronstedtite	Rivkin et al. (2006), Milliken and Rivkin (2009)
Magnetite	Larson et al. (1979), Milliken and Rivkin (2009) and Rivkin et al. (2011)

Notes: Formulas of minerals are shown in Table 3.
[a] Magnesite and/or dolomite.

Ceres' spectra have no distinct signatures of many primary minerals (olivine, pyroxenes, feldspars) and Mg-rich phyllosilicates (saponite, serpentine), which are common in chondrites. Although spectral features of these minerals in the near-IR could be masked by opaque phases, mid-IR spectra are not consistent with a presence of these phases (Rivkin et al., 2006; Milliken and Rivkin, 2009). The apparent absence or deficiency of primary phases indicates through alteration of primary materials. Fe-bearing carbonates and calcite may not be abundant (Milliken and Rivkin, 2009). Sulfates are not seen, though chlorides may not be detected in visible to mid-IR spectral ranges. Although there are no clear spectral signatures of organic compounds in Ceres' spectra, absorptions of aromatic groups at 3.3–3.4 μm (Moroz et al., 1998; Rivkin et al., 2006) could be overlapped by carbonate bands (Milliken and Rivkin, 2009; Rivkin et al., 2011).

The nature of the prominent absorption feature at ~3.06 μm remains uncertain. The interpretation of this feature as a sign of water frost (Lebofsky et al., 1981) is not supported in subsequent

Table 3
Minerals and their standard Gibbs free energies of formation, $\Delta_f G^0$ (25 °C, 1 bar).

Mineral	Formula	Abbreviation	$\Delta_f G^0$ (kJ/mol)	Reference
Magnetite	Fe_3O_4	Mt	−1012.3	HP98
Greenalite	$Fe_3Si_2O_5(OH)_4$	Gr	−2993.0	H78
Fe–Mg serpentine	$(Fe_{0.6}Mg_{0.4})_3Si_2O_5(OH)_4$	Fe–Mg-sp	−3409.8	MZ
Chrysotile	$Mg_3Si_2O_5(OH)_4$	Chr	−4030.7	HP98
Cronstedtite	$Fe^{2+}{}_2Fe^{3+}{}_2SiO_5(OH)_4$	Crn	−2613.4[d]	WJ04
			−2618.4[e]	V8R6
			−2619.2	THER
			−2606.6	W10
Mg–Fe cronstedtite[a]	$Fe^{2+}{}_{0.4}Mg_{1.6}Fe^{3+}{}_2SiO_5(OH)_4$	Mg–Fe-crn	−3170.9	MZ
Mg-cronstedtite	$Mg_2Fe^{3+}{}_2SiO_5(OH)_4$	–	−3308.7	WOL
Goethite	FeOOH	gth	−490.6	N08
Ferrihydrite	$Fe(OH)_3$[c]	fr	−711.0	N08
Amorph. SiO_2[b]	SiO_2	SiO_2(am)	−848.9	H78
Brucite	$Mg(OH)_2$	br	−834.3	HP98
Magnesite	$MgCO_3$	ms	−1027.8	H78
Siderite	$FeCO_3$	sid	−679.5	H78
Talc	$Mg_3Si_4O_{10}(OH)_2$	tlc	−5516.7	HP98
Fe-talc	$Fe_3Si_4O_{10}(OH)_2$	FeTlc	−4451.1	HP98

[a] The Mg–Fe cronstedtite corresponds to the composition of a most Mg-rich phase reported in literature with Mg/(Mg + Fe) = 0.4 (Zega and Buseck, 2003).
[b] Quartz is not considered because it is absent from carbonaceous chondrites.
[c] The nominal formula used here.
[d] The value used in calculations of equilibrium constants and phase diagrams (Table 4, Figs. 1–4).
[e] The value used in calculations of chemical equilibria by the Gibbs free energy minimization method (Figs. 5–7). HP98, Holland and Powell (1998); H78, Helgeson et al. (1978); MZ, the energy was evaluated assuming ideal mixing between Mg and Fe end members; WJ04, Wolery and Jove-Colon (2004); V8R6, the LLNL database "termo_com_V8R6+" (1996) from the GWB site (http://www.gwb.com); THER, the database "thermo_dat.txt" (1986) from the GWB site; W10, Wilson (2010); WOL, evaluated by Thomas Wolery; N08, Navrotsky et al. (2008). Thermodynamic properties of aqueous species were from Shock et al. (1989, 1997).

works (King et al., 1992; Rivkin et al., 2011). The ice-free materials are consistent with the instability of ice at the surface (Fanale and Salvail, 1989) and with the lack of detection of water vapor emission from Ceres (Rousselot et al., 2011; Küppers et al., 2012). A presence of NH_4-bearing saponite clay with the 3.06 μm feature (King et al., 1992) is inconsistent with Ceres' mid-IR spectra (Rivkin et al., 2006; Milliken and Rivkin, 2009). Milliken and Rivkin (2009) demonstrated that brucite is a reasonable candidate for the 3.06 μm feature and is consistent with Ceres' spectra at 3–14 μm. However, the 3.06 μm feature may not be the fundamental brucite band (Pascale et al., 2004; Beck et al., 2011a,b) and some brucite bands are not clearly seen in Ceres' spectra at 1–3 μm. The deeper depths of the 'brucite' (3.06 μm) and 'carbonate' (3.3–3.4 and 3.8–3.9 μm) bands in darker regions disagree with a low albedo of these minerals and remain unexplained (Rivkin and Volquardsen, 2010).

Despite these uncertainties, a mixture of Mg-bearing carbonates, brucite, cronstedtite, and magnetite provides a good fit for Ceres' spectra at 3–14 μm (Milliken and Rivkin, 2009). It is the most reliable current model for Ceres' surface mineralogy (Rivkin et al., 2011). This model indicates some similarity of Ceres' materials with CM carbonaceous chondrites which contain these aqueously formed phases (Brearley and Jones, 1998; Brearley, 2006a). Major differences between CM chondrites and Ceres' materials are apparently abundant carbonates and brucite on Ceres and a deficiency of other minerals of CM chondrites (Mg–Fe serpentine, tochilinite, troilite, etc.). These differences could reflect specific aqueous environments on Ceres and/or parent planetesimals. A similarity of Ceres' spectra with some spectra of 10 Hygiea and 324 Bamberga (e.g., Takir and Emery, 2012) imply analogous aqueous processes on these three large low-density bodies (Table 1).

Initial interpretations of Ceres' surface mineralogy suggested actions of alkaline CO_2-bearing aqueous fluids at moderately oxidizing conditions (Li et al., 2006; Milliken and Rivkin, 2009; Rivkin and Volquardsen, 2010; Rivkin et al., 2011). However, specific chemical pathways and geological contexts of aqueous processes remain to be evaluated. In this paper, we consider chemical equilibria in aqueous environments to investigate formation conditions of Ceres' minerals. Major attention is devoted to cronstedtite, brucite, and Mg carbonates. The discussion is based on the assumption that the identification of theses minerals is correct. Our conclusions about the formation of brucite are based on the assumption that Mg–Fe serpentine is not present. We discuss the results in terms of geological evolution and internal structure of Ceres and suggest other minerals which could be present.

2. Terrestrial/chondritic occurrences and stabilities of minerals

In this section, we review occurrences of cronstedtite and brucite, evaluate their stability, and discuss formal chemical pathways of their formation. We develop phase diagrams with stability fields of minerals as functions of activities of dissolved species (SiO_2, Mg^{2+}, etc.), fugacities of gases (fH_2, fCO_2), and temperature (T) at 1 bar total pressure (P). This is done through calculations of equilibrium constants of chemical reactions that include chemical species of interest. Equilibrium constants are calculated from Gibbs free energies of species at standard conditions (Tables 3 and 4). In addition to phase diagrams, we report evaluations of cronstedtite stability performed through calculations of chemical equilibria in the multicomponent chondrite–water–gas type system.

2.1. Cronstedtite-bearing assemblages

On Earth, cronstedtite is a rare phyllosilicate that contains ferric and ferrous iron (Table 3) (Deer et al., 1963). However, cronstedtite is abundant in fine-grained matrices and chondrule rims of CM carbonaceous chondrites. Investigations of CM chondrites indicate that formation of cronstedtite is related to aqueous oxidation of kamacite in the presence of dissolving silicates which provide aqueous SiO_2 (e.g., Tomeoka and Buseck, 1985; Zolensky and McSween, 1988; Beck et al., 2012), as illustrated by overall reaction

$$4Fe^0\ (\text{metal}) + SiO_2(aq) + 7H_2O(l) \rightarrow Fe^{2+}{}_2Fe^{3+}{}_2SiO_5(OH)_4 + 10H_2. \quad (33)$$

Meteoritic cronstedtite contains a significant amount of Mg, and the Mg/(Fe+Mg) atomic ratio could reach 0.4 (e.g., Zega and Buseck, 2003). Cronstedtite is less abundant in more altered CM chondrites, reflecting the replacement of cronstedtite by Fe–Mg serpentine as alteration progresses (Tomeoka and Buseck, 1985; Browning et al., 1996; Zega and Buseck, 2003; Rubin et al., 2007; Howard et al., 2011). In addition to Fe–Mg serpentine, cronstedtite coexists with tochilinite. Magnetite is not a major secondary phase in CM chondrites, it forms together with cronstedtite and after it (Brearley and Jones, 1998; Howard et al., 2011; Beck et al., 2012). Oxygen and carbon isotopic data for CM's carbonates and other evaluations indicate alteration at $T < \sim 30$ °C (Clayton and Mayeda, 1999; Benedix et al., 2003; Guo and Eiler, 2007; Zolensky et al., 1989, 1993). These data suggest that cronstedtite also forms at low temperatures.

2.1.1. Thermodynamic stability of cronstedtite

Thermodynamic properties of cronstedtite have not been measured and estimated standard Gibbs free energies of formation ($\Delta_f G^0$) differ from each other (Table 3). Although the stability of cronstedtite cannot be evaluated with accuracy based on current data, the topology of Fe–Si–O–H system and broad effects of fH_2, temperature, and activity of dissolved SiO_2, $aSiO_2(aq)$, on cronstedtite stability could be assessed. For calculation of equilibrium constants and corresponding activity diagrams, we use $\Delta_f G^0$ data from Wolery and Jove-Colon (2004). Our evaluations of cronstedtite stability with use of activity diagrams are in general agreement with results of Dyl et al. (2006, 2010) and Dyl (2011) who used data from the LLNL database.

The relative stability of cronstedtite and Fe-serpentine (greenalite) could be illustrated by reaction (1) in Table 4. Cronstedtite forms at more oxidizing conditions (lower fH_2) and lower activities of dissolved silica than greenalite. Reactions (2) and (3) show that cronstedtite forms at more reducing conditions than magnetite and goethite (at fixed $aSiO_2(aq)$). A narrow stability field of cronstedtite is confined by fH_2 and $aSiO_2(aq)$ values set by equilibrium constants of reactions (1)–(3) (Fig. 1a). However, goethite is not common in chondrites, while ferrihydrite occurs in CI, CM, and some other types of carbonaceous chondrites (Brearley and Jones, 1998; Wasson and Rubin, 2010; Beck et al., 2012). Ferrihydrite is stable at $fH_2 < \sim 10^{-23}$ (Eq. (4)). If ferrihydrite is considered instead of goethite, the stability fields of magnetite and cronstedtite become broader and cronstedtite coexists with magnetite and/or Fe-serpentine in a wide range of fH_2 and $aSiO_2(aq)$ conditions (Fig. 1b). Cronstedtite forms at elevated activities of $SiO_2(aq)$ within the stability field of talc. However, at high $aSiO_2(aq)$ values, the stability field of cronstedtite could be limited at $aSiO_2(aq)$ values that correspond to saturation with respect to amorphous silica (Eq. (5)). The Mg-rich cronstedtite could be stable at slightly higher fH_2 and $aSiO_2(aq)$ values than pure cronstedtite (Eq. (1a); Fig. 1b).

Eq. (6) illustrates precipitation reaction of cronstedtite which includes Fe^{2+} supplied by dissolving metal, sulfide, or silicate phases and protons released together with H_2. At alkaline pH, typical for chondritic aqueous systems (e.g., Zolensky et al., 1989; Rosenberg et al., 2001), cronstedtite coexists with a Fe^{2+}-poor solution (Fig. 2). Higher concentrations of Fe^{2+} are needed to stabilize

Table 4
Chemical reactions and their equilibrium constants at 1 bar.

	Reaction	$\log_{10}K$, 25 °C	$\log_{10}K$, 75 °C
(1)	$3crn + 5SiO_2(aq) + 3H_2 = 4gr + H_2O$	35.4	27.5
(1a)	$3\ Mg–Fe\text{-}crn + 5SiO_2(aq) + 3H_2 = 4Fe–Mg\text{-}sp + H_2O$	34.5	–
(2)	$3crn = 4mt + 3SiO_2(aq) + H_2 + 5H_2O$	−18.4	−13.7
(3)	$crn + H_2O = 4gth + SiO_2(aq) + H_2$	−9.61	−7.29
(4)	$mt + 5H_2O = 3fr + 0.5H_2$	−11.4	–
(5)	$SiO_2(am) = SiO_2(aq)$	−2.72	−2.32
(6)	$4Fe^{2+} + SiO_2(aq) + 7H_2O = crn + 8H^+ + H_2$	−43.2	−34.5
(7)	$chr + H_2O = 3br + 2SiO_2(aq)$	−17.2	−14.6
(8)	$tlc + H_2O = chr + 2SiO_2(aq)$	−9.88	−8.44
(9)	$gr + 2SiO_2(aq) = FeTlc + H_2O$	4.99	4.31
(10)	$gr + 4H_2O + 3mt + SiO_2(aq) = 3crn$	4.95	3.43
(11)	$3gr + 5mt + 7H_2O = 6crn + H_2$	−3.53	−3.45
(12)	$gr = mt + 2SiO_2(aq) + H_2O + H_2$	−13.4	−10.3
(13)	$3crn + 13SiO_2(aq) + 3H_2 = 4FeTlc + 5H_2O$	55.3	44.8
(14)	$FeTlc = mt + 4SiO_2(aq) + H_2$	−18.4	−14.6
(15)	$gr + H_2O = 3gt + 2SiO_2(aq) + 1.5H_2$	−16.1	−12.3
(16)	$FeTlc + 2H_2O = 3gt + 4SiO_2(aq) + 1.5H_2$	−21.0	−16.7
(17)	$mt + 2H_2O = 3gth + 0.5H_2$	−2.61	−2.03
(18)	$mt + 3CO_2 + H_2 = 3sid + H_2O$	14.1	8.09
(19)	$crn + 4CO_2 + H_2 = 4sid + SiO_2(aq) + 3H_2O$	12.7	6.21
(20)	$FeTlc + 3CO_2 = 3sid + 4SiO_2 + H_2O$	−4.33	−6.54
(21)	$gr + 3CO_2 = 3sid + 2SiO_2(aq) + 2H_2O$	0.66	−2.22
(22)	$crn + CO_2 = sid + mt + SiO_2(am) + 2H_2O$	1.28	1.89
(23)	$3Fe^0 + 4H_2O = mt + 4H_2$	11.2	11.8
(24)	$Fe_3P + 8H_2O + 3H^+ = mt + PO_4^{3-} + 9.5H_2$	–	–
(25)	$br + CO_2 = ms + H_2O$	6.37	4.41
(26)	$chr + 3CO_2 = 3\ ms + 2SiO_2(aq) + 2H_2O$	−1.91	−1.41
(27)	$tlc + 3CO_2 = 3\ ms + 4SiO_2(aq) + H_2O$	−7.97	−9.85
(28)	$2chr + 3CO_2 = tlc + 3\ ms + 3H_2O$	11.7	6.98
(29)	$br + 2H^+ = Mg^{2+} + 2H_2O$	16.5	13.7
(30)	$chr + 6H^+ = 3Mg^{2+} + 2SiO_2(aq) + 5H_2O$	32.3	26.4
(31)	$tlc + 6H^+ = 3Mg^{2+} + 4SiO_2(aq) + 4H_2O$	22.4	18.0
(32)	$Mg^{2+} + CO_2 + H_2O = ms + 2H^+$	−10.1	−9.28

Note: Abbreviations for minerals are shown in Table 3. H_2O designates liquid water, H_2 and CO_2 are gases, and $SiO_2(aq)$ stands for dissolved silica.

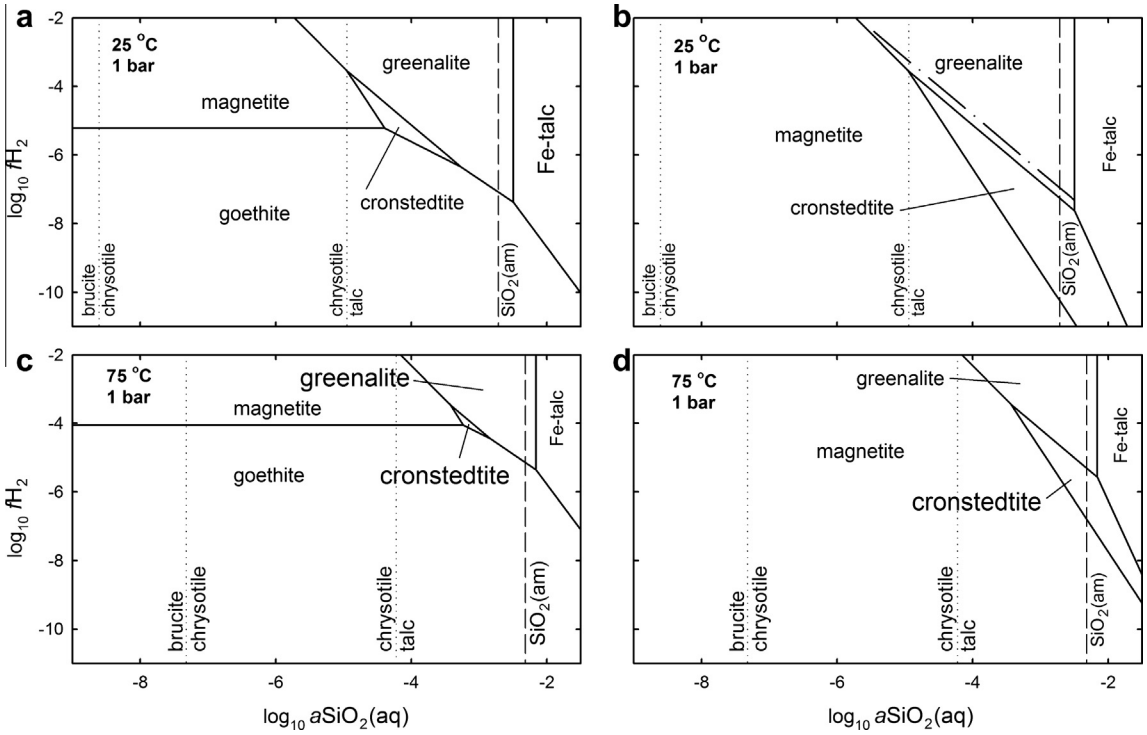

Fig. 1. The stability fields of minerals in the Fe–Si–O–H system as functions of fH_2 and $aSiO_2(aq)$ at 25 °C (a and b) and 75 °C (c and d). In (a and c), goethite is considered stable ferric iron phase. In (b and d), ferrihydrite is the stable ferric iron phase (forms at $fH_2 < \sim 10^{-23}$ at 25 °C, Eq. (4)). The lines correspond to equilibrium conditions of reactions (1)–(17) in Table 4. In (b), the dash-dotted line corresponds to equilibrium between Mg–Fe cronstedtite and Fe–Mg serpentine (Eq. (1a)). The vertical dashed lines correspond to $aSiO_2(aq)$ at solution saturation with respect to amorphous SiO_2 (Eq. (5)). This saturation limits stabilities of cronstedtite and greenalite and makes Fe-talc a metastable phase. The vertical dotted lines correspond to $aSiO_2(aq)$ values set by Eqs. (7) and (8).

cronstedtite at lower pH and $aSiO_2$, and at higher fH_2. At constant fH_2 and $aSiO_2$, formation of cronstedtite could be driven by increases in pH and/or aFe^{2+}.

The stability of cronstedtite decreases as temperature increases. At 75 °C, cronstedtite is stable within a very limited set of conditions (Fig. 1c and d). At 0 °C, cronstedtite forms in a wide range of redox conditions, especially if dissolved SiO_2 is saturated with respect to amorphous SiO_2 (Fig. 3a). At $T < \sim 25$ °C, it could also form at $aSiO_2(aq)$ as low as $\sim 10^{-6}$, close to $aSiO_2$ values at the chrysotile–talc equilibrium (Eq. (8)) (Fig. 3b). These results show that cronstedtite may not form at $T > \sim 120$ °C at any fH_2 and $aSiO_2(aq)$. Dyl (2011) reports that cronstedtite may not form at $T > \sim 50$ °C.

Conditions for carbonation of Fe-bearing minerals depend on redox conditions, temperature, and $aSiO_2(aq)$ (Fig. 4). At 25 °C, cronstedtite could be subjected to carbonation to siderite (Eq. (19)) at $fCO_2 > \sim 10^{-3}$ bars. As temperature increases, higher fCO_2 values are needed and cronstedtite becomes more stable with respect to carbonation (Figs. 3c and 4c). The fCO_2 values at the cronstedtite–magnetite–siderite equilibrium (Eq. (22); Fig. 3c) set an upper limit for fCO_2 during the formation of cronstedtite-bearing and $FeCO_3$-less mineralogies seen on Ceres and CM chondrites. Carbonation of Mg silicates and brucite may occur at much lower fCO_2 which should not affect cronstedtite (Fig. 3c).

In addition to development of phase diagrams, we calculated chemical equilibria in the 17-element water–chondrite–gas system at temperature 0–150 °C and 1 bar total pressure. The calculations were performed by the Gibbs free energy minimization method with the GEOCHEQ code and database (Mironenko et al., 2008) previously used and described in Zolotov et al. (2006) and Zolotov (2012). For bulk rock compositions, we used the water-free composition of CM carbonaceous chondrites (Lodders and Fegley, 1998) with 20% of carbon participating in chemical reactions. The rest of C was assumed chemically inert, reflecting a dominance of the insoluble organic matter in carbonaceous chondrites. These calculations allowed us to evaluate molar amounts of formed minerals, concentrations and activities of dissolved species in aqueous solution, and amounts, concentrations and fugacities of gases in equilibrium with other components of the system. We explored effects of $\Delta_f G^0$ of cronstedtite, water/rock (W/R) mass ratio, temperature, and fH_2 on the amount of cronstedtite formed. Formation of cronstedtite was observed only if the $\Delta_f G^0$ is less than the value from Wolery and Jove-Colon (2004) (Fig. 5). We used the $\Delta_f G^0$ data from the LLNL 1996 database (Table 3) in these calculations, which complement the results obtained from activity diagrams (Figs. 1–4). The results show that cronstedtite forms below ~70 °C only at high W/R ratios (Figs. 5–7). Cronstedtite does not coexist with serpentine and/or saponite only at very high W/R ratios ($>\sim 10^6$) (Fig. 6). At lower temperature, cronstedtite forms in a wider range of W/R ratios (Figs. 6 and 7). At 0 °C, it forms at the W/R ratio as low as 2.5. Low temperature also favors formation of cronstedtite in a wide range of fH_2 (Fig. 7), consistent with the diagrams shown in Figs. 1 and 3a. At 0 °C, the majority of cronstedtite forms at fH_2 = ~10^{-6} to 10^{-1} and W/R = ~10^7 to ~5.

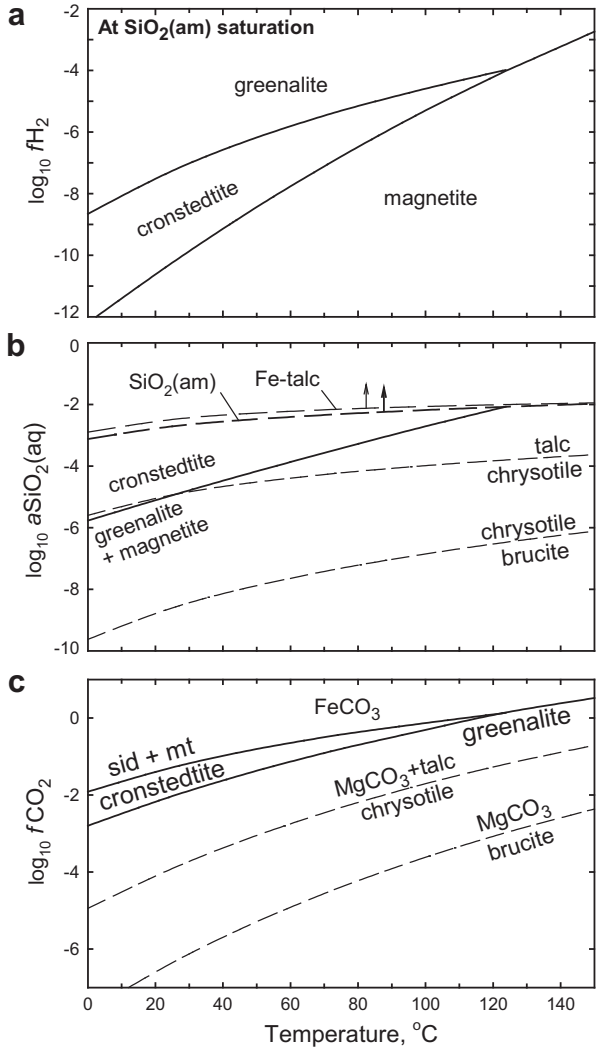

Fig. 3. The stability fields of minerals as functions of temperature, fH_2, $aSiO_2(aq)$, and fCO_2. In (a), the curves correspond to Eqs. (1), (2) and (12) at solution saturation with respect to SiO_2(am). In (b), the solid curve corresponds to Eq. (10). The thin dashed curve shows the field of metastable Fe-talc limited by Eq. (9) within the stability field of SiO_2(am). Other dashed curves correspond to Eqs. (7) and (8). In (c), the solid curves refer to Eqs. (21) and (22) at SiO_2(am) saturation. Dotted curves refer to Eqs. (25) and (28). At temperature < 100 °C, pressure is 1 bar. At higher temperatures, pressure corresponds to that of water–gas saturation.

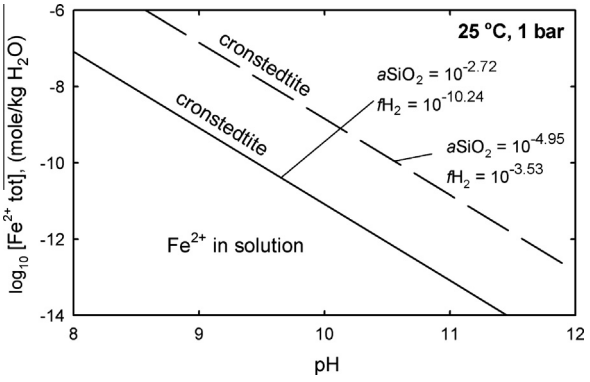

Fig. 2. The equilibrium conditions of cronstedtite dissolution as functions of pH and total Fe^{2+} content in solution at 25 °C. The solid line is for Eq. (6) at solution saturation with respect to SiO_2(am) and at fH_2 set by the cronstedtite–magnetite equilibrium (Eq. (2)) at SiO_2(am) saturation (Eq. (5)). The dashed line is for Eq. (6) at $aSiO_2(aq)$ and fH_2 set by the cronstedtite–greenalite–magnetite Eqs. (10) and (11), respectively. These lines show upper and lower ranges of cronstedtite stability.

2.1.2. Formation of cronstedtite in carbonaceous chondritic materials

The formation of cronstedtite at high W/R ratios and low-T, high-$aSiO_2(aq)$, and low-fH_2 conditions could reflect a specific stage of aqueous alteration of chondritic materials. Melting of water ice on carbonaceous asteroids should have prevented the temperature increase above ~0 °C over a period of time. A prolonged coexistence of liquid water in the presence of partially melted ice (cf., Grimm and McSween, 1989; Wilson et al., 1999)

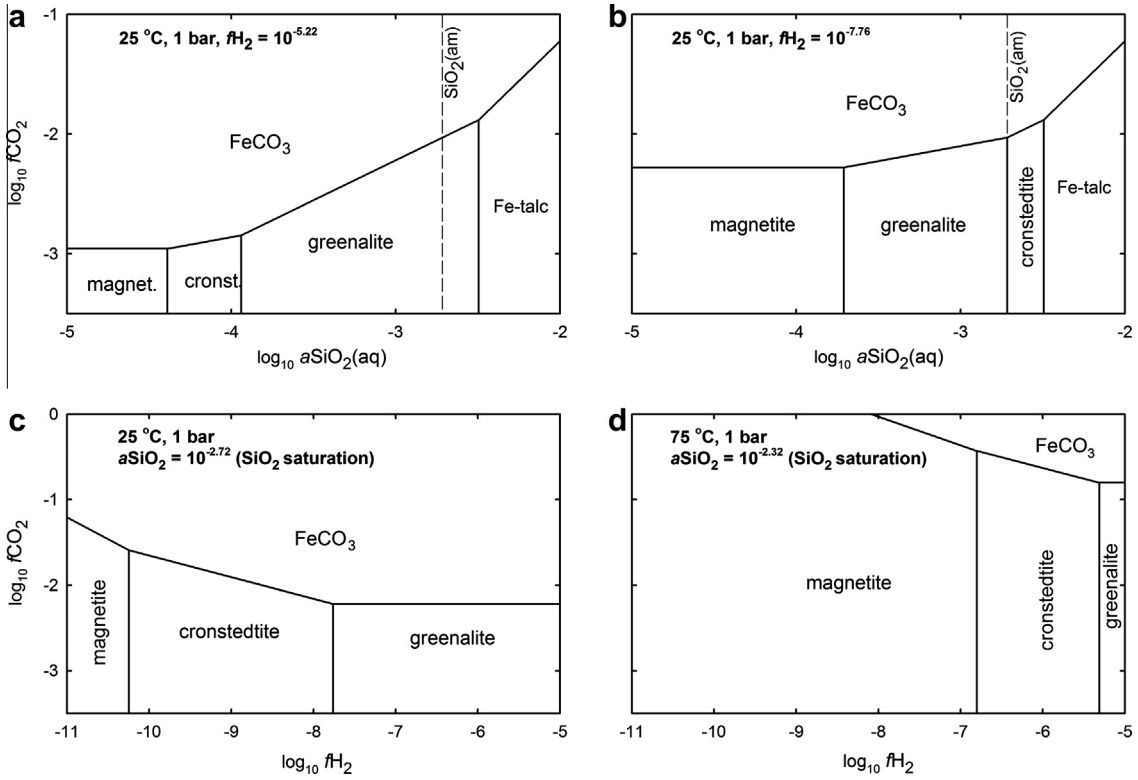

Fig. 4. The stability fields of minerals in the Fe–Si–O–H–C system as functions of fH_2 and fCO_2 at 25 °C (a–c) and 75 °C (d). The solid lines correspond to Eqs. (18–22). In (a), at fH_2 set by the magnetite–goethite equilibrium (Eq. (17)). In (b), at fH_2 set by the cronstedtite–greenalite equilibrium (Eq. (1)) at SiO_2(am) saturation. In (c and d), at solution saturation with respect to SiO_2(am).

suggests formation of cronstedtite at that early stage of alteration. The high W/R mass ratios needed for precipitation of cronstedtite could reflect a large amount of liquid water reacted with a small fraction of a rock, independent of bulk W/R ratio in the system, which may not be higher than ~0.5 in typical asteroidal materials. Decreasing W/R ratio could be used a proxy for alteration progress (alteration is completed when the W/R ratio becomes equal to bulk W/R ratio at ~0.2–0.5). An elevated activity of SiO_2(aq) at early stages of alteration could be accounted for by rapid dissolution of amorphous silicate materials, which are abundant in primitive chondrites (Brearley and Jones, 1998; Wasson and Rubin, 2010). Relatively low fH_2 values that characterize cronstedtite formation (Figs. 3a and 7) may also characterize very early stages of aqueous alteration when only a small amount of H_2 is produced through oxidation of reducing Fe phases by water (Eqs. (23) and (24)). Low fH_2 values indicate that H_2 does not form its own gas phase and that H_2 is only a minor component of a H_2O-rich gas phase, if it exists. The low activity of dissolved H_2 (aH_2(aq) = ~10^{-9} at fH_2 = ~10^{-6}) could reflect a large amount of liquid water reacted with a small fraction of a reduced rock. In addition to early stages

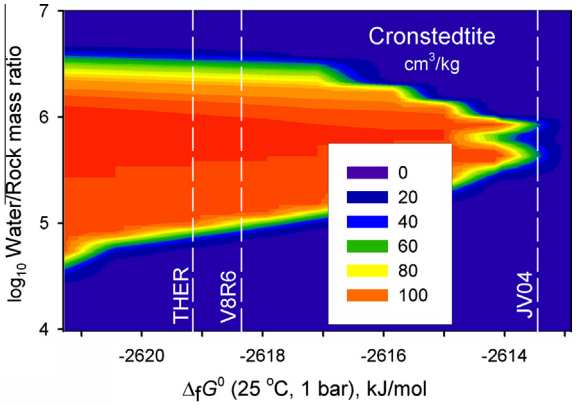

Fig. 5. The volume of cronstedtite (cm^3) formed through alteration of 1 kg of anhydrous rock with the composition of anhydrous CM chondrite as a function of Gibbs free energy of formation of cronstedtite at 25 °C and 1 bar total pressure. H_2 fugacity is fixed at 10^{-3}. The vertical dashed lines correspond to the formation energies depicted in Table 3.

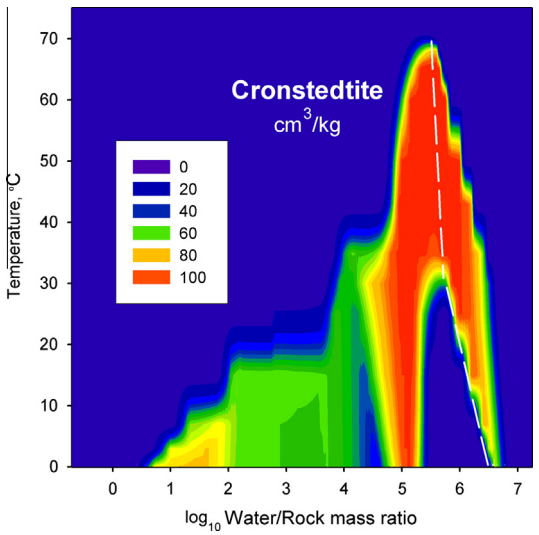

Fig. 6. The volume of cronstedtite (cm^3) formed through alteration of 1 kg of anhydrous CM chondrite as a function of temperature and W/R ratio. To the right-hand side off the dashed lines, cronstedtite does not form together with Mg–Fe serpentine or saponite.

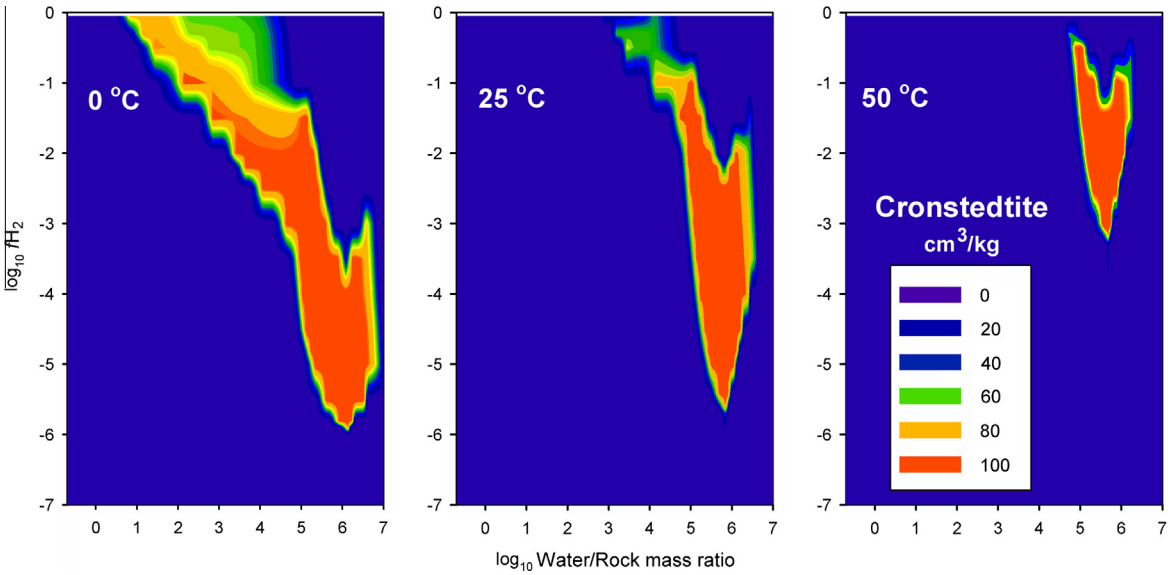

Fig. 7. The volume of cronstedtite formed through alteration of 1 kg of anhydrous CM chondrite as a function of H_2 fugacity and *W*/*R* ratio at three different temperatures.

of alteration, low-fH_2 environments may characterize transient low-*P* aqueous solutions at near-boiling conditions which may characterize shallow subsurface environments on internally heated and/or impacted asteroids. The inferences about formation of cronstedtite at low fH_2 at early stages of alteration or in low-*P* open system environments are consistent with findings of Dyl (2011) and Rosenberg et al. (2001).

As alteration progresses, production of H_2 through oxidation of kamacite and schreibersite may lead to the formation of H_2-rich gas phase, which affects total pressure, especially in low-permeability and low-porosity materials (e.g., Wilson et al., 1999; Rosenberg et al., 2001). Activity of SiO_2 in solution may decrease as alteration progresses, reflecting dissolution of olivine grains and precipitation of low-solubility Mg-serpentine. A supply of Fe^{2+} from dissolving primary Fe-bearing phases may decrease as well. These and other changes (e.g., in *pH* and temperature) affected stability of cronstedtite. In particular, an increase in fH_2 favors the cronstedtite to serpentine conversion, which has not fully occurred in CM chondrites (e.g., Howard et al., 2011) and may have not occurred in Ceres' surface materials. Although a decrease in $aSiO_2$(aq) is not required for this conversion, it is a possible alteration trend in CM chondrites (Fig. 8). A presence of putative cronstedtite–magnetite assemblage on Ceres (Milliken and Rivkin, 2009) suggests changes in fH_2 and $aSiO_2$(aq) along the phase boundary of cronstedtite and magnetite (Fig. 8). This path implies more oxidizing conditions during formation of that assemblage on Ceres (lower pressure and fH_2) than on parent bodies of CM chondrites.

2.2. Brucite-bearing assemblages

On Earth, brucite forms through aqueous alteration of Mg-rich rocks and minerals in a wide range of temperatures in pressures (Deer et al., 1963; Hostetler et al., 1966; Moody, 1976a; Hemley et al., 1977). In olivine-rich rocks, such as dunites, it forms through serpentinization reaction

$$2Mg_2SiO_4\ (\text{in olivine}) + 3H_2O(l) \rightarrow Mg(OH)_2 + Mg_3Si_2O_5(OH)_4\ (\text{Mg-serpentine}) \quad (34)$$

Chrysotile (Mg-serpentine) and brucite readily form through near-surface serpentinization of olivine-rich peridotites (Barnes et al., 1978). Brucite typically contains a $Fe(OH)_2$ component, which is more abundant in low-*T* serpentinites with a low magnetite content (Moody, 1976a,b). Another common reaction of brucite formation is hydrolysis of periclase (MgO) in marbles and thermally metamorphosed Mg-rich limestones and schists exposed to aqueous solutions or steam,

$$MgO + H_2O \rightarrow Mg(OH)_2. \quad (35)$$

Brucite does not commonly form during aqueous alteration of chondrites. Zolensky et al. (1993) reported individual grains and vein fillings of Mg–Fe brucite in association with serpentine and saponite in heated CI chondrite Y-82162. Some brucite-type layers with basal spacing of ~4.8 Å were seen in fine-grained matrices of CM chondrites (Mackinnon and Buseck, 1979; Barber, 1981, 1985) and as a component of tochilinite structure (Mackinnon and Zolensky, 1984). Barber (1985) noticed a Fe-rich composition of brucite-type layers in CM chondrites, consistent with a low-*T* alteration. However, individual brucite phases may not be present in CM chondrites. Formation of brucite layers, especially interlayering of Mg-serpentine with brucite (Mackinnon and Buseck, 1979), may characterize microenvironments (cf., Brearley, 2006b)

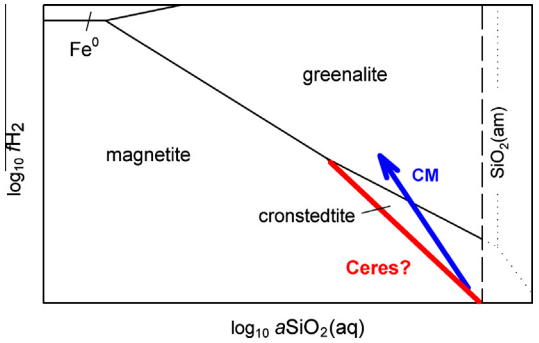

Fig. 8. Possible alteration pathways in Ceres' materials and CM chondrites plotted on the schematic stability diagram of Fe-bearing minerals. The dotted lines show the mineral stability fields within the stability field of amorphous SiO_2 (see Fig. 1a and b). A putative Ceres' path shows changes in fH_2 and $aSiO_2$(aq) along with the cronstedtite–magnetite phase boundary. The CM's path illustrates that the observed conversion of cronstedtite to serpentine could be driven by increasing fH_2 and a decrease in activity of dissolved SiO_2. fH_2 increases because of oxidation of Fe-metal (in kamacite) and schreibersite by liquid water (Eqs. (23) and (24)).

with an elevated Mg/Si atomic ratio related to alteration of forsterite, Mg_2SiO_4. The paucity of brucite in chondrites is consistent with the low Mg/Si ratio in carbonaceous chondrites (~1.04, Lodders and Fegley, 1998), reflecting comparable amounts of forsterite and Mg-rich pyroxene accreted on their parent bodies. In contrast to terrestrial dunites, serpentinization in chondrites is roughly characterized by reaction

$$Mg_2SiO_4\ (\text{in olivine}) + MgSiO_3\ (\text{in pyroxene}) + 2H_2O(l) \rightarrow Mg_3Si_2O_5(OH_4)\ (\text{in serpentine}), \quad (36)$$

though a significant amount of Fe incorporates in serpentine from altering kamacite, schreibersite, troilite, and anhydrous ferrous silicates, and additional SiO_2(aq) is supplied from other silicate materials. This reaction also illustrates terrestrial alteration of pyroxene-rich (>40% pyroxene) peridotites which leads to brucite-free serpentinites (Hostetler et al., 1966). It follows that formation of abundant brucite in Ceres' materials requires olivine-rich rocks (Milliken and Rivkin, 2009), other putative solids with an elevated Mg/Si ratio, or specific aqueous conditions.

The stability of brucite in natural low-T aqueous environments is mainly controlled by reactions that involve Mg^{2+}, OH^-, SiO_2(aq), and inorganic C species. The key reaction of brucite formation

$$Mg^{2+} + 2OH^- \rightarrow Mg(OH)_2 \quad (37)$$

implies that either high aMg^{2+} or aOH^- (high pH) are needed to precipitate brucite (Fig. 9). At concentrations of Mg^{2+} evaluated for reduced (sulfate-less) solutions in CI carbonaceous chondrites (~10^{-5}–10^{-8} mole/kg H_2O, Zolotov (2012)), brucite may form at pH > ~10.5. As examples, brucite precipitates through interaction of hydroxyl-rich (NaOH-type, NH_4OH-type) solutions and Mg^{2+}-bearing fluids or Mg salts (chlorides, sulfates or carbonates). As temperature increases, brucite becomes stable at lower pH and/or aMg^{2+} values (Fig. 9), though stability of brucite decreases at T > ~370 °C (Hemley et al., 1977).

Brucite forms only at very low activities of dissolved SiO_2 (<~10^{-9} at T < 20 °C). The upper $aSiO_2$(aq) limit of brucite stability is determined by the chrysotile–brucite equilibrium (Eq. (7), Figs. 1, 3b, and 10). Formation of brucite could be driven by a decrease in $aSiO_2$(aq), if other parameters (pH, aMg^{2+}, fCO_2) are suitable. In chondritic materials, such a decrease could be due to alteration of olivine following dissolution of amorphous SiO_2-rich materials. However, in silicate-rich CI/CM-type chondritic materials with a low bulk Mg/Si ratio, $aSiO_2$(aq) should not be below values set by the brucite–chrysotile equilibrium (Eq. (7)). The coexistence of brucite and chrysotile in terrestrial serpentinization environments and the chrysotile–brucite interlayering in CM chondrites implies local $aSiO_2$(aq) values close to those equilibrium values. Note that

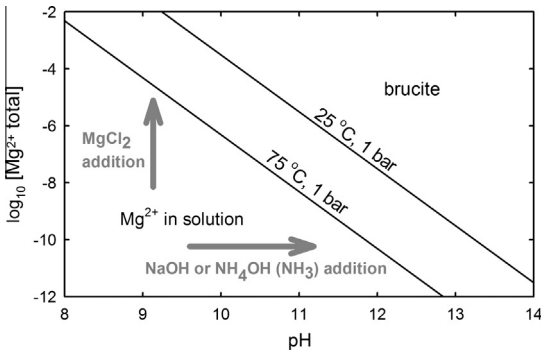

Fig. 9. The stability field of brucite as functions of pH and total Mg^{2+}concentration in solution. The lines correspond to Eq. (29). The arrows show exemplary pathways that facilitate formation of brucite.

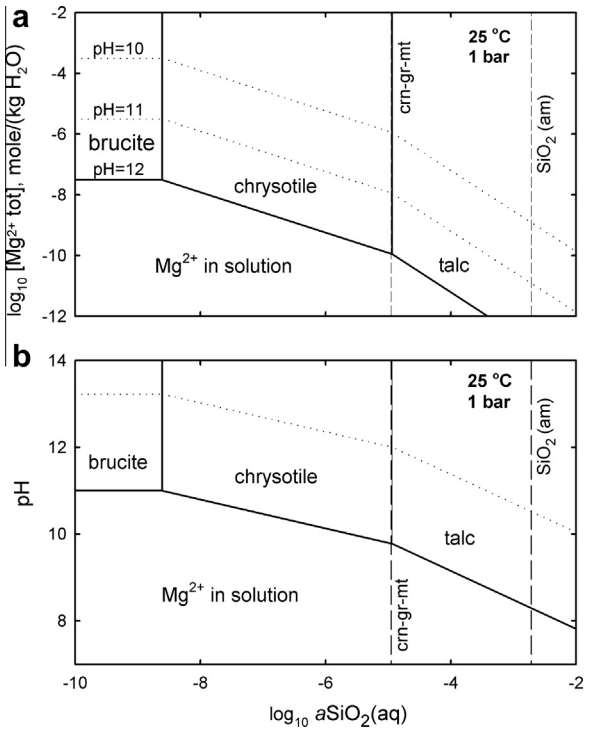

Fig. 10. The stability fields of minerals in the Mg–Si–O–H system as functions of pH and $aSiO_2$(aq) at 25 °C. The solid lines correspond to Eqs. (7), (8), and (29)–(31). The vertical dashed lines refer to $aSiO_2$ set by Eqs. (5) and (10). In (a), solid lines correspond to equilibrium conditions at pH = 12, and dotted lines corresponds to pH = 11 and 10. In (b), the solid lines are for the total Mg^{2+} concentration of $10^{-5.51}$ mole/kg H_2O which corresponds to brucite dissolution at pH = 11 (Eq. (29)). The dotted lines are for the Mg^{2+}concentration of $10^{-9.95}$ mole/kg H_2O set by Eqs. (30) or (31) at aSO_2(aq) controlled by the chrysotile-talc equilibrium (Eq. (8)) at pH = 12.

$aSiO_2$(aq) values set by Eq. (7) are much less than those that correspond to stabilities of cronstedtite, talc, greenalite, and amorphous silica (Figs. 3b and 10). It follows that brucite cannot form in equilibrium with these phases.

In addition to high pH and low $aSiO_2$(aq) values, a stable existence of brucite requires low activities of dissolved carbonate species (HCO_3^-, CO_3^{2-}) which prevent formation of Mg carbonates. Fugacity of CO_2 should also be low to have a high pH. The brucite–magnesite equilibrium (Eq. (25)) sets an upper limit for fCO_2 that allows the stability of brucite (Fig. 3c, Figs. 11 and 12). At

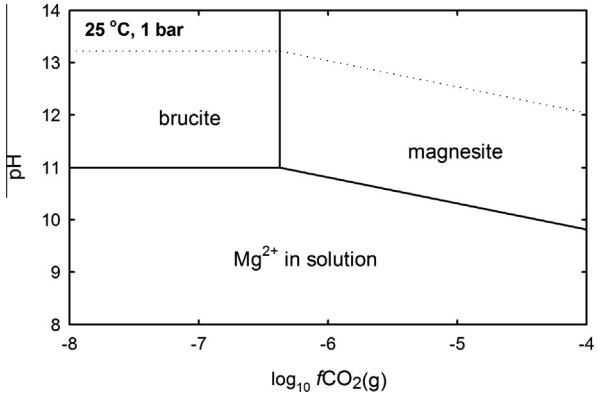

Fig. 11. The stability fields of minerals in the Mg–O–H–C system as functions of pH and $aSiO_2$(aq) at 25 °C. For solid and dotted lines, concentrations of Mg^{2+} are depicted in the caption of Fig. 10b. The lines correspond to Eqs. (25), (29), and (32).

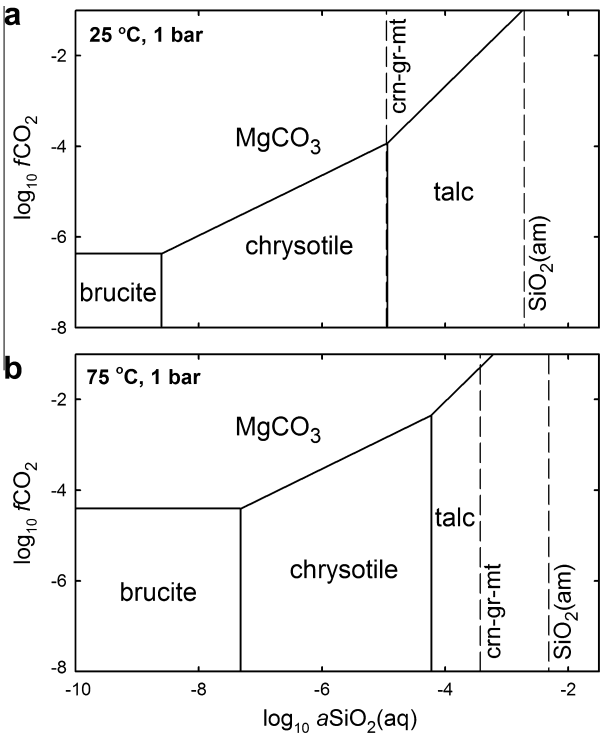

Fig. 12. The stability fields of minerals in the Mg–Si–O–H system as functions of fCO_2 and $aSiO_2$(aq) at 25 °C (a) and 75 °C (b). The solid lines refer to Eqs. (7), (8), and (25)–(27). The vertical dashed lines correspond to aSO_2(aq) at SiO_2(am) saturation and at the cronstedtite–greenalite–magnetite equilibrium (Eq. (10)). The plot shows that brucite is much vulnerable for carbonation than Mg silicates.

25 °C, the Eq. (25) corresponds to $fCO_2 = 10^{-6.4}$ bars. This value is three orders of magnitude lower than fCO_2 in the Earth's atmosphere, which accounts for a rapid carbonation of brucite exposed at the surface (Hostetler et al., 1966; Mumpton and Thompson, 1966, 1975). On asteroids, the low fCO_2 value set by Eq. (25) could characterize low-pressure conditions of shallow subsurface. A coexistence of brucite with magnesite may indicate their formation at fCO_2 values close to those set by Eq. (25).

3. Discussion: Origin of Ceres' surface minerals

The aqueous mineralogy of Ceres' surface could reflect the composition of accreted materials modified by endogenic and exogenic processes, and impacts. Formation conditions of some minerals may not (and need not) be related to formation of other minerals. A plausible formation scenario for surface minerals needs to be consistent with the instability of aqueous solutions in the vicinity of Ceres' surface, with the assumed lack or paucity of olivine, pyroxenes, feldspars, serpentine, saponite, and sulfates, with an elevated abundance of Mg-bearing carbonates and brucite, and with a low albedo and a small spectral contrast of porous clay-like surface materials (Section 1.1).

3.1. Origin of cronstedtite

An occurrence of cronstedtite in Ceres' surface materials indicates aqueous alteration of rocky materials similar to those accreted on parent bodies of CM carbonaceous chondrites (kamacite, forsterite, enstatite, amorphous silicates, Ca–Al oxides, troilite, organic matter, etc.) together with water-rich ices. Ices could have melted on parent planetesimals and on Ceres through thermal processes in their interiors and impacts.

A formation of cronstedtite on planetesimals implies their accretion within several Myr after the formation of Ca–Al-rich inclusions (CAI) to have enough ^{26}Al to melt ices. Elevated porosities of small planetesimals favored low-P and low-fH_2 conditions needed for formation of cronstedtite. Modestly altered CM chondrites with elevated cronstedtite/serpentine ratios (Murchison, Murray, Mighei, and Nogoya; Howard et al., 2011) could be compositional analogs of such planetesimals. The formation of cronstedtite on parent planetesimals agrees with a model of undifferentiated Ceres accreted from hydrated planetesimals similar to CI/CM chondrites (Zolotov, 2009). A detection of serpentine, tochilinite, unaltered silicates, and kamacite in Ceres' materials will be consistent with a formation of cronstedtite on planetesimals. However, the planetesimal model may not explain abundant carbonates and brucite and the apparent lack of serpentine on Ceres.

Neither water ice nor aqueous solutions are stable at current low-P and low-T (<∼−30 °C) conditions of Ceres' surface (Fanale and Salvail, 1989). If they are warmed and wetted, near-surface materials could be feasible for transient aqueous alteration and cronstedtite formation at low-P conditions that favor H_2 escape. However, thermal evolution models do not indicate ice melting in upper parts of the Ceres' interior (McCord and Sotin, 2005; Castillo-Rogez and McCord, 2010; Castillo-Rogez, 2011). Near-surface aqueous processes driven by internal heating may require major thermal dehydration of the Ceres' deep interior, inconsistent with the low density of the body (Table 1). A strong heating by short-lived radioactivity would have led to formation of water mantle and a submergence of a primordial rocky shell into water layer (McCord and Sotin, 2005).

In a case of differentiated Ceres, aqueous processes may not be possible in a cold rocky shell above putative icy mantle, even if such a crust survives. A rock–ice interface above icy mantle cannot be warmed by internal thermal processes to cause local ice melting and aqueous alteration of the rock. Aqueous minerals (phyllosilicates, magnetite, carbonates, etc.) formed at the bottom on an early water ocean may not be delivered to the surface. A downward freezing of oceanic water should have accumulated a layer of oceanic salts above altered rocky core. Putative convection in water mantle (frozen ocean) would supply mainly oceanic salts, which are not observed at the surface. It follows that the presence of cronstedtite and other aqueous phases at the surface may not be satisfactorily explained by thermal processes in the Ceres' interior. However, local warming of Ceres by impacts could have led to precipitation of cronstedtite from cold fluids in the vicinity of the body's surface. Impact processes could have been responsible for the formation of other surface minerals, as discussed below.

3.2. Origin of brucite

Although serpentinization of olivine is a common path to form brucite, Ceres' brucite may not be related to alteration of olivine-rich rock. An early spectroscopic sign of olivine on Ceres (Witteborn et al., 2000) has not been confirmed. There are no olivine-rich chondrites with the Mg/Si atomic ratio of ∼2 (Lodders and Fegley, 1998), consistent with Mg/Si = 1 in the solar photosphere (Lodders, 2003). On Earth and Mars, dunites and other olivine-rich peridotites form through igneous processes which should not have occurred in upper parts of the Ceres' interior. Alteration of Mg-rich olivine is accompanied by the formation of Mg-serpentine, as seen in serpentinites and chrysotile–brucite interlaying in chondrites (Section 2.2). The lack of observational evidence of Mg-serpentine on Ceres is inconsistent with the formation of brucite through alteration of olivine.

Brucite does not form together with cronstedtite because much different activities of SiO_2(aq) are needed for precipitation of these

minerals. It is also unlikely that these minerals precipitated sequentially from solution with evolving concentration of dissolved SiO_2 because such an evolution could have led to deposition of Mg-serpentine. If follows that brucite, if it is present, could have precipitated from transient SiO_2-poor fluids or formed through hydrolysis of MgO (Eq. (35)).

A formation of transient brucite-forming fluids on large asteroids is more likely than on planetesimals. Neither small asteroids nor chondrites demonstrate a presence of abundant brucite. Brucite-poor CM/CI chondrites reveal isochemical alteration without fluid migration (Bland et al., 2009). However, gravity of large bodies favors motions of fluids (Young et al., 2003; Travis and Schubert, 2005), especially in permeable outer parts of their interiors. Large bodies such as Ceres are better suited for preservation of heat of short-lived radioactive elements and could be fairly warmed by long-lived radioactivity (McCord and Sotin, 2005; Castillo-Rogez and McCord, 2010; Castillo-Rogez, 2011). Massive bodies are also more vulnerable to high-velocity impacts followed by transient aqueous processes at late stages of accretion and subsequent events, such as Late Heavy Bombardment (LHB) which affected terrestrial planets, the Moon, and asteroids (Gomes et al., 2005; Marchi et al., 2013). The presence of the 'brucite' spectral signature on other two large asteroids (Table 1; Takir and Emery, 2012) could be related to *in situ* aqueous processes as well.

In Ceres' near-surface environments, brucite could have precipitated from cold short-lived Mg-bearing solutions which did not interact with preexisting silicates. Mg-rich fluids could be presented by sulfate and/or chloride solutions, which could exist at subzero temperatures in the Ceres' interior, consistent with occurrences of Mg–Na–Cl–SO_4 type fluids on parent bodies CI and CM chondrites (Fanale et al., 2001; Izawa et al., 2010). However, the lack of sulfate spectral features in surface materials and stronger effects of chlorides on the depression of freezing point of water makes the $MgCl_2$-type fluids more likely than the $MgSO_4$-type.

In addition to sources of Mg^{2+}, abundant hydroxyl is needed for aqueous deposition of brucite (Eq. (37)). There are at least two mechanisms to form OH-rich fluids. NaOH-type fluids may form if Na-bearing silicates (e.g., smectites) do not precipitate, as it was suggested for parent bodies of saponite-deficient CR carbonaceous chondrites (Zolotov, 2012). In such a case, an abundant Na^+ ion in solution is compensated by OH^- formed through dissociation of water. The apparent lack of saponite in Ceres' surface materials does not contradict to an occurrence of such fluids. However, NaOH-type solutions freeze at higher temperature than pure water and may not be delivered to the cold Ceres' surface. Another way to form OH-rich fluids is hydrolysis of ammonia, $NH_3 + H_2O(l) \rightarrow NH_4^+ + OH^-$. Ceres-forming planetesimals could have contained NH_3 even if they formed in the main asteroid belt (Dodson-Robinson et al., 2009). Accretion of NH_3-bearing compounds on some carbonaceous asteroids is consistent with the detection of NH_3 in products of hydrous pyrolysis of CR chondrites (Pizzarello et al., 2011). Accretion of NH_3 was more likely if carbonaceous asteroids formed beyond the current orbit of Jupiter (Walsh et al., 2011) and if Ceres initially formed as a trans-Neptunian object (McKinnon, 2008, 2012). Metastable NH_4OH-type fluids (NH_3 solutions in water) could exist at $T > -98$ °C in Ceres' subsurface. However, an occurrence and mobility of NH_3-bearing fluids is limited in carbonate-rich systems because of precipitation of ammonium carbonates (Kargel, 1992; Marion et al., 2012). Sings of ammoniated salts (e.g., NH_4Cl, NH_4HCO_3, $(NH_4)_2CO_3$) and silicates (cf., King et al., 1992) in Ceres' materials will validate processes that involved NH_3.

In the vicinity of Ceres' surface, brucite may form through interaction of OH-rich fluids with preexisting Mg-bearing solutions or salts (e.g., $MgCl_2$, $MgCO_3$, $MgSO_4$) by reactions

$$2OH^- + MgCO_3 \rightarrow Mg(OH)_2 + CO_3^{2-} \quad (38)$$

$$2OH^- + MgCl_2 \rightarrow Mg(OH)_2 + 2Cl^- \quad (39)$$

$$2OH^- + MgSO_4 \rightarrow Mg(OH)_2 + SO_4^{2-}. \quad (40)$$

These reactions show that formation of brucite could be followed by deposition of carbonates, chlorides, or sulfates of Na^+ or NH_4^+. A detection of one of these minerals in association with brucite will constrain a pathway of brucite formation.

Although transient near-surface fluids could be generated by impacts, OH-rich and SiO_2-poor fluids may not be formed. However, brucite could form through hydrolysis of MgO and Mg^0 by steam in cooling impact plumes. High pressures increase the stability of brucite; it can be equilibrium with MgO (Eq. (35)) at 1250 °C and 15 GPa (Johnson and Walker, 1993). Both MgO and Mg^0 form through dissociation of silicates, as seen in high-*T* evaporation experiments and models (e.g., Markova et al., 1986; de Niem et al., 2008; Berezhnoy, 2010, 2013). $Mg(OH)_2$ is modeled as the main Mg condensate of lunar H-bearing impact gases (Berezhnoy, 2010, 2013). These inferences are consistent with results of laser-induced impact experiments with silicates in water-rich environments that show the formation of Mg-OH and Fe-OH bonds, and corresponding phyllosilicates in condensates (Gerasimov et al., 1994a, 2002). The impact formation of brucite on Ceres may indicate water-rich conditions in the target and could be consistent with the differentiated body with outer water (ice) shell at the time of bombardment.

3.3. Origin of Mg carbonates

The apparent higher abundance of Ceres' carbonates than in CI/CM chondrites and a negative carbonate-albedo correlation (Section 1.1) suggest *in situ* origin. Carbonates may signify Ceres' origin in the outer Solar System and/or indicate accretion of cometary materials which may contain up to ~30 mol% of C oxides relative to H_2O (A'Hearn et al., 2012) and much organic compounds. Though, the strong spectral features of carbonates may reflect coating of mineral grains rather than a high abundance.

Carbonates could have formed though boiling, outgassing, evaporation, and freezing of aqueous solutions that briefly appeared at the surface. Deposition of carbonates could be driven by CO_2 degassing from fluids exposed to low-*P* environments in the vicinity of Ceres' surface. The corresponding reaction

$$(Ca, Mg)^{2+} + 2HCO_3^- \rightarrow (Ca, Mg)CO_3 + H_2O(l) + CO_2(g) \quad (41)$$

is responsible for deposition of carbonates in terrestrial springs and soils, and may account for precipitation in a shallow subsurface on Mars (Niles et al., 2009). The common inhibition of aqueous precipitation of Mg carbonates (magnesite, dolomite) at ambient temperatures (Lippmann, 1973) may indicate disequilibrium and/or high-*T* deposition of these carbonates on Ceres. As an example, deposition in a dynamic environment could lead to zoned carbonate globules with Ca-rich cores and Mg-rich exteriors. Such a zoning is seen in the ALH 84001 martian carbonate (e.g., Harvey and McSween, 1996; Niles et al., 2009) formed at 14–22 °C (Halevy et al., 2011). A similar deposition on Ceres suggests that Ca carbonates could be present but not seen. At slightly elevated fCO_2, various Mg carbonates may also form through alteration of brucite (e.g., Eq. (25)) as it happens at the Earth's surface (Mumpton and Thompson, 1966, 1975). In addition, Mg carbonates and brucite could have precipitated together. Alkaline low-*T* conditions favor the formation of OH-bearing and hydrated Mg carbonates. Hydromagnesite, $Mg_5(CO_3)_4(OH)_2{\cdot}4H_2O$, artinite, $Mg_2(CO_3)(OH)_2{\cdot}3H_2O$, and nesquehonite, $Mg(HCO_3)(OH){\cdot}2H_2O$, often coexist with brucite and may contribute to spectral features of Ceres' surface.

Formation of surface carbonates could be related to processes in the interior (e.g., thermal oxidation of organic matter and CO_2 degassing, Rivkin et al., 2011) and impacts. However, percolation of interior fluids rich in inorganic C species is less likely than chloride-, Mg/Na sulfate-, or NH_3-bearing solutions because of an early precipitation of low-solubility carbonates from fluids subjected to freezing or evaporation. The lack of detection of soluble salts is more consistent with a formation of Ceres' carbonates from organic species oxidized in impacts. An impact formation of carbonates could involve CO_2(g) interaction with condensates in cooling plumes (Gerasimov et al., 1994b, 2002), and aqueous precipitation in impact-generated clouds, fluidized crater outflows, and temporal ice-covered lakes. Abundant carbonates may reflect exceptionally C- and H_2O-rich projectiles from outer Solar System collided with Ceres. Addition views about the role of impacts are presented in the following section.

3.4. Impact formation of surface materials

Surfaces of asteroids, they orbits and families, together with samples from parent bodies of chondrites, indicate numerous collisions over the Solar System history. Models show that Ceres could have been impacted ~4600 times by main belt asteroids with the diameter (D) > 1 km, and 47 impact craters with D > 100 km is expected (de Elía and Di Sisto, 2011). In addition to these evaluations, multiple collisions with C- and H_2O-rich bodies external to the main asteroid belt are expected during LHB (Marchi et al., 2013; Brož et al., 2013). Round albedo details on Ceres (Li et al., 2006; Carry et al., 2008) and B type members of the 10 Hygiea family (Mothé–Diniz et al., 2001) are consistent with major collisions on these bodies. The age of the Hygiea family asteroids (2 ± 1 Gyr) is consistent with post-accretional collisions (Brož et al., 2013). The low spectral contrast of Ceres (e.g., Carry et al., 2012) and Hygiea (Mothé–Diniz et al., 2001) could reflect impact homogenization by impact surges and gravitational fallout of ejected materials, which may not be efficient on smaller asteroids. The fine-grained (dusty) and porous surface materials on Ceres (Section 1.1) and Hygiea (Lebofsky et al., 1985; Johnston et al., 1989) could be gravitationally-sorted impact deposits.

As noted above, aqueous minerals could form in cooling impact plumes (Gerasimov et al., 1994a, 1994b, 2002), fluidized crater outflows, transient ice-covered crater lakes and related low-T hydrothermal systems (Ivanov and Pierazzo, 2011). An enhanced partial pressure of H_2O in impact gases increases both the temperature stability of hydrated minerals and rates of hydration, as discussed for putative shock waves in ice-bearing regions of the solar nebula (Ciesla et al., 2003). An impact origin has been discussed for martian aqueous minerals (Tornabene et al., 2013) and Ceres' impact-driven processes could be somewhat similar to those on early water-rich martian regolith. On Ceres, the current mineralogy could represent lag deposits after sublimation of ice from near-surface regolith, if near-surface ice was left after the bombardment.

Both high-T dissociation of silicates, water molecules, and Fe^0–H_2O interaction led to oxidizing environments in impact plumes and deposits (e.g., Gerasimov et al., 2002; Ciesla et al., 2003). Escape of reduced gases (H_2, CH_4 and light hydrocarbons) and trapping of CO_2 and O_2 in carbonates and oxides contributed to overall oxidation. Ferrous and ferric phases (e.g., magnetite, cronstedtite) formed through oxidation of Fe-metal. Some sulfide S could be oxidized to S^0 and sulfates (Zolotov and Mironenko, 2007). Carbon oxides and abundant carbonates formed through ample oxidation of organic matter. Possible deficiency of organic species in Ceres' surface materials (Rivkin et al., 2011) together with abundant oxidized species may indicate prevailed oxidation and exceptionally water-rich targets. However, partially altered and/or impact-generated soot-like organic compounds (cf., Gerasimov et al., 2002) could be among species that make Ceres' surface darker.

Contrast chemical environments and chemical disequilibria in turbulent impact plumes and surges may lead to the formation of minerals which typically do not form together (e.g., cronstedtite and brucite; carbonates and organics). It is possible that phyllosilicates (cronstedtite) form in craters and outflows from post-impact SiO_2-bearing fluids, while brucite form predominantly in impact plumes. A rapid consumption of Mg in brucite and carbonates may limit formation of Mg-serpentine and saponite.

On Ceres, water-rich targets imply a bombardment of an icy shell formed through water–rock differentiation (McCord and Sotin, 2005) before LHB. The nondetection of high-solubility salts is more consistent with mineral deposition by impact-generated than percolated interior fluids. On differentiated Ceres, salts could be accumulated at the bottom of icy mantle (Section 3.1). In such a case, salt-less aqueous minerals form through transient alteration of materials of icy targets and rock-bearing impactors. Impact-generated surface composition may not characterize the interior composition of differentiated body. Although the impact origin of surface minerals is in agreement with differentiated Ceres, mineral-forming processes during collisions of an undifferentiated and hydrated Ceres with water-rich bodies during LHB remain a possibility.

The apparent similarity of surface mineralogy of three bodies with different sizes (Table 1) may indicate major effects of exogenic processes. On Hygiea, both low density and highly oblate spheroid shape (Ragazzoni et al., 2000) do not signify thermal dehydration of rocks and do not exclude an ice-bearing interior. A similarity of near-IR and mid-IR spectra of Hygiea with spectra of some thermally metamorphosed CI/CM and CO chondrites (Hiroi et al., 1996; Barucci et al., 2002) may indicate impact-induced alteration of surface mineralogy. Collisions with an ice-bearing Bamberga could have contributed to its surface mineralogy as well.

4. Concluding remarks

The unusual spectra of Ceres, 10 Hygiea, and 324 Bamberga in the ultraviolet to mid-IR spectral regions imply unique processes that formed surface materials on these bodies. The strong hydration feature in the 3 μm region implies formation of surface minerals in water-rich environments. However, the instability of liquid water at the surface's cold and low-pressure conditions suggests the formation of aqueous minerals in the interior, near the surface by transient fluids, and/or on parent planetesimals.

Cronstedtite forms at elevated W/R ratios in moderately oxidized low-T aqueous environments which may characterize early stages of alteration of CM-type chondritic planetesimals and upper parts of the Ceres' interior. A formation of Ceres' cronstedtite on CM-type planetesimals may not be consistent with undetection of other secondary minerals of CM chondrites. In the deep interior, alteration by immobile fluids at low W/R ratios and elevated H_2 pressures may not lead to cronstedtite-rich rocks. Hydration of silicates in the upper parts of Ceres may require a major thermal dehydration of the deep interior, inconsistent with the low density of the body. However, cronstedtite could form from near-surface fluids generated by impacts.

Brucite and carbonates are minor minerals in chondrites altered in interiors of their parent bodies and these minerals may not be abundant deep in the Ceres' interior. A formation of abundant brucite below the surface requires a unique olivine-rich composition, which may not be explained with known mineralogy of primitive meteorites. The apparent absence of Mg-rich serpentine from surface materials is inconsistent with origin of brucite through serpentinization of olivine. Brucite is not stable with respect to Mg

carbonates and silicates at elevated fCO_2 and $aSiO_2$(aq) which may characterize conditions in the deep interior. Low-pressure open-system environments with elevated W/R ratios and mobile fluids are better suitable for formation of brucite and carbonates. Both minerals were rather deposited from temporary fluids than formed though a gradual alteration of silicate rocks in the vicinity of Ceres' surface. Near-surface conditions allow accumulation of solids precipitated from transient fluids through their low-pressure boiling, degassing, evaporation, and/or freezing. Carbonates could form before, after or together with brucite.

A formation of Ceres' surface minerals through percolation of interior fluids is inconsistent with the lack of detection of high-solubility salts. Both carbonate (HCO_3^-, CO_3^{2-}) bearing and OH-rich fluids may not percolate toward the cold surface of undifferentiated Ceres. Interior fluids may not reach the surface if an icy mantle exists. Therefore, we argue for origin of surface minerals in impact jets, fluidized crater outflows, and related low-T hydrothermal systems. Regardless of icy mantle, the unique surface composition could be related to post-accretional bombardment of ice-bearing Ceres, possibly during LHB that affected parent asteroids of many meteorites. 10 Hygiea and 324 Bamberga could have experienced similar processes. An idealized impact model suggests evaporation of olivine and Mg pyroxene to form MgO gases and condensates followed by rapid MgO consumption in reactions with H_2O and CO_2 to form brucite and Mg carbonates, respectively. The consumption of MgO may limit formation of Mg phyllosilicates. Cronstedtite and magnetite form in oxidizing conditions that correspond to water-rich targets. Abundant carbonates reveal an efficient oxidation of organic matter. The observed clay-type and spatially homogeneous surface materials could be gravitationally sorted deposits of impact clouds. The impact hypothesis will gain a support if fluidized crater outflows and impact surge deposits are observed, though earlier deposits of aqueous minerals could have been obliterated and homogenized. A detection and mapping of salts and other aqueous minerals with Dawn instruments will constrain aqueous processes on Ceres. Data on surface mineralogy will complement Dawn gravity, topography, and compositional information to constrain the internal structure and geological history of Ceres.

Acknowledgments

This work is supported by Grants from NASA Planetary Geology and Geophysics, Cosmochemistry, and Outer Planet Research programs, and NASA Astrobiology Institute. The author appreciates comments from two thoughtful reviewers and conversations with Julie Castillo-Rogez, Ralph Milliken, Thomas Wolery, Katie Dyl, and Mikhail Mironenko, who is thanked for earlier calculations related to the stability of cronstedtite.

References

A'Hearn, M.F. et al., 2012. Cometary volatiles and origin of comets. Astrophys. J. 758 (1), 8 pp. (article ID 29).
Baer, J., Chesley, S.R., Matson, R.D., 2011. Astrometric masses of 26 asteroids and observations on asteroid porosity. Astron. J. 141 (5), 12 pp. (article ID 143).
Barber, D.J., 1981. Matrix phyllosilicates and associated minerals in C2M carbonaceous chondrites. Geochim. Cosmochim. Acta 45, 945–970.
Barber, D.J., 1985. Phyllosilicates and other layer-structured materials in stony meteorites. Clay Miner. 20, 415–454.
Barnes, I., O'Neil, J.R., Trescases, J.J., 1978. Present day serpentinization in New Caledonia, Oman and Yugoslavia. Geochim. Cosmochim. Acta 42, 144–145.
Barucci, M.A. et al., 2002. 10 Hygiea: ISO infrared observations. Icarus 156, 202–210.
Beck, P. et al., 2011a. Goethite as an alternative origin of the 3.1 μm band on dark asteroids. Astron. Astrophys. 526, A85. http://dx.doi.org/10.1051/0004-6361/201015851.
Beck, P. et al., 2011b. Goethite as an alternative origin of the 3.1 μm band on dark asteroids (Corrigendum). Astron. Astrophys. 530, C2. http://dx.doi.org/10.1051/0004-6361/201015851e.
Beck, P. et al., 2012. The redox state of iron in the matrix of CI, CM and metamorphosed CM chondrites by XANES spectroscopy. Geochim. Cosmochim. Acta 99, 305–316.
Benedix, G.K. et al., 2003. Carbonates in CM2 chondrites: Constraints on alteration conditions from oxygen isotopic compositions and petrographic observations. Geochim. Cosmochim. Acta 67, 1577–1588.
Berezhnoy, A.A., 2010. Meteoroid bombardment as a source of the lunar exosphere. Adv. Space Res. 45, 70–76.
Berezhnoy, A.A., 2013. Chemistry of impact events on the Moon. Icarus 226, 205–211.
Bland, P.A. et al., 2009. Why aqueous alteration in asteroids was isochemical: High porosity ≠ high permeability. Earth Planet. Sci. Lett. 287, 559–568.
Brearley, A.J., 2006a. The action of water. In: Lauretta, D.S., McSween, H.Y., Jr. (Eds.), Meteorites and Early Solar System II. University of Arizona Press, Tucson, pp. 587–624.
Brearley, A.J., 2006b. The role of microchemical environments in the alteration of CM carbonaceous chondrites. Lunar Planet. Sci. 37. Abstract 2074.
Brearley, A.J., Jones, R.H., 1998. Chondritic meteorites. In: Papike, J.J. (Ed.), Planetary Materials, Rev. Mineral., vol. 36, Miner. Soc. Amer., Washington, DC, pp. 1–398.
Browning, L.B., McSween Jr., H.Y., Zolensky, M.E., 1996. Correlated alteration effects in CM carbonaceous chondrites. Geochim. Cosmochim. Acta 60, 2621–2633.
Brož, M., Morbidelli, A., Bottke, W.F., Rozehnal, J., Vokrouhlický, D., Nesvorný, D., 2013. Constraining the cometary flux through the asteroid belt during the late heavy bombardment. Astron. Astrophys. 551, A117, arXiv:1301.6221 [astro-ph.EP].
Carry, B., 2012. Density of asteroids. Planet. Space Sci. 73, 98–118.
Carry, B. et al., 2008. Near-infrared mapping and physical properties of the dwarf-planet Ceres. Astron. Astrophys. 478, 235–244.
Carry, B. et al., 2012. The remarkable surface homogeneity of the Dawn mission target (1) Ceres. Icarus 217, 20–26.
Castillo-Rogez, J.C., 2011. Ceres – Neither a porous nor salty ball. Icarus 215, 599–602.
Castillo-Rogez, J.C., McCord, T.B., 2010. Ceres: Evolution and present state constrained by shape data. Icarus 205, 443–459.
Chamberlain, M.A., Lovell, A.J., Sykes, M.V., 2009. Submillimeter photometry and light curves of Ceres and other large asteroids. Icarus 202, 487–501.
Ciesla, F.J., Lauretta, D.S., Cohen, B.A., Hood, L.L., 2003. A nebular origin for chondritic fine-grained phyllosilicates. Science 299, 549–552.
Clayton, R.N., Mayeda, T.K., 1999. Oxygen isotope studies of carbonaceous chondrites. Geochim. Cosmochim. Acta 63, 2089–2104.
de Elía, G.C., Di Sisto, R.P., 2011. Impactor flux and cratering on Ceres and Vesta: Implications for the early Solar System. Astron. Astrophys. 534, 7 pp. (ID A129).
de Niem, D., Kührt, E., Motschmann, U., 2008. Initial condensate composition during asteroid impacts. Icarus 196, 539–551.
Deer, W.A., Howie, R.A., Zussman, J., 1963. Rock-forming Minerals. Longmans, London.
Dodson-Robinson, S.E., Willacy, K., Bodenheimer, P., Turner, N.J., Beichmana, C.A., 2009. Ice lines, planetesimal composition and solid surface density in the solar nebula. Icarus 200, 672–693.
Dyl, K.A., 2011. Correlating Oxidation and Oxygen Isotopic Composition to Nebular and Parent Body Processes in Chondritic Meteorites. Ph.D. Thesis, University of California, Los Angeles.
Dyl, K.A., Manning, C.E., Young, E.D., 2006. Modeling aqueous alteration of CM carbonaceous chondrites: Implications for cronstedtite formation by water–rock reaction. Lunar Planet. Sci. 37. Abstract 2060.
Dyl, K.A., Manning, C.E., Young, E.D., 2010. The implications of cronstedtite formation in water-rich planetesimals and asteroids. In: Astrobiology Sci. Conf. Abstract 5627.
Fanale, F.P., Salvail, J.R., 1989. The water regime of asteroid 1 Ceres. Icarus 82, 97–110.
Fanale, F.P. et al., 2001. An experimental estimate of Europa's "ocean" composition independent of Galileo orbital remote sensing. J. Geophys. Res. 106 (E7), 14595–14600.
Feierberg, M.A., Lebofsky, L.A., Larson, H.P., 1981. Spectroscopic evidence for aqueous alteration products on the surfaces of low-albedo asteroids. Geochim. Cosmochim. Acta 45, 971–981.
Gerasimov, M.V., Dikov, Yu.P., Yakovlev, O.I., Wlotzka, F., 1994a. Water-vapor trapping from the atmosphere by condensed silicate material produced during pulsed evaporation. Geochem. Int. 31 (11), 135–146.
Gerasimov, M.V., Dikov, Yu.P., Yakovlev, O.I., Wlotzka, F., 1994b. Trapping of carbon dioxide from a hot atmosphere by condensing silicates. Lunar Planet. Sci. 25, 415–416.
Gerasimov, M.V., Dikov, Yu.P., Yakovlev, O.I., Wlotzka, F., 2002. Experimental investigation of the role of water in impact vaporization chemistry. Deep-Sea Res. II 49, 995–1009.
Gomes, R., Levison, H.F., Tsiganis, K., Morbidelli, A., 2005. Origin of the cataclysmic late heavy bombardment period of the terrestrial planets. Nature 435, 466–469.
Grimm, R.E., McSween Jr., H.Y., 1989. Water and the thermal evolution of carbonaceous chondrite parent bodies. Icarus 82, 244–280.
Guo, W., Eiler, J.M., 2007. Temperatures of aqueous alteration and evidence for methane generation on the parent bodies of the CM chondrites. Geochim. Cosmochim. Acta 71, 5565–5575.
Halevy, I., Fischer, W.W., Eiler, J.M., 2011. Carbonates in the Martian meteorite Allan Hills 84001 formed at 18 ± 4 °C in a near-surface aqueous environment. Proc. Natl. Acad. Sci. USA 108, 16895–16899.

Harvey, R.P., McSween, H.Y., 1996. A possible high-temperature origin for the carbonates in the martian meteorite ALH84001. Nature 382, 49–51.
Helgeson, H.C., Delany, J., Bird, D.K., 1978. Summary and critique of the thermodynamic properties of rock-forming minerals. Am. J. Sci. 278A, 1–229.
Hemley, J.J., Montoya, J.W., Christ, C.L., Hostetler, P.B., 1977. Mineral equilibria in the MgO–SiO_2–H_2O system: I Talc–chrysotile–forsterite–brucite stability relationship. Am. J. Sci. 277, 322–351.
Hiroi, T., Pieters, C.M., Zolensky, M.E., Lipschutz, M.E., 1995. Thermal metamorphism of the C, G, B, and F asteroids seen from the 0.7 μm absorption band in comparison with carbonaceous chondrites. Antarct. Meteorit. 20, 72–75.
Hiroi, T., Zolensky, M.E., Pieters, C.M., Lipschutz, M.E., 1996. Thermal metamorphism of the C, G, B, and F asteroids seen from the 0.7 μm, 3 μm, and UV absorption strengths in comparison with carbonaceous chondrites. Meteorit. Planet. Sci. 31, 321–327.
Holland, T.J.B., Powell, R., 1998. An internally consistent thermodynamic data set for phases of petrologic interest. J. Metamorph. Geol. 16, 309–343.
Hostetler, P.B., Coleman, R.G., Mumpton, F.A., Evans, B.W., 1966. Brucite in Alpine serpentinites. Am. Mineral. 51, 75–98.
Howard, K.T., Benedix, G.T., Bland, P.A., Cressey, G., 2011. Modal mineralogy of CM chondrites by X-ray diffraction (PSD-XRD): Part 2. Degree, nature and settings of aqueous alteration. Geochim. Cosmochim. Acta 75, 2735–2751.
Ivanov, B.A., Pierazzo, E., 2011. Impact cratering in H_2O-bearing targets on Mars: Thermal field under craters as starting conditions for hydrothermal activity. Meteorit. Planet. Sci. 46, 601–619.
Izawa, M.R.M., Nesbitt, H.W., Macrae, N.D., Hoffman, E.L., 2010. Composition and evolution of the early oceans: Evidence from the Tagish Lake meteorite. Earth Planet. Sci. Lett. 298 (3–4), 443–449.
Johnson, M.C., Walker, D., 1993. Brucite [$Mg(OH)_2$] dehydration and the molar volume of H_2O to 15 GPa. Am. Mineral. 78, 271–284.
Johnston, K.J. et al., 1989. The microwave spectra of the asteroids Pallas, Vesta, and Hygiea. Astron. J. 98, 335–340.
Kargel, J.S., 1992. Ammonia–water volcanism on icy satellites: Phase relations at 1 atmosphere. Icarus 100, 556–574.
King, T.V.V., Clark, R.N., Calvin, W.M., Sherman, D.M., Brown, R.H., 1992. Evidence for ammonium-bearing minerals on Ceres. Science 255, 1551–1553.
Kovačevič, A.B., 2012. Determination of the mass of Ceres based on the most gravitationally efficient close encounters. Mon. Not. R. Astron. Soc. 419, 2725–2736.
Küppers, M. et al., 2012. Search for water vapour emission from Dawn Target (1) Ceres with Herschel. Asteroids, Comets, Meteors 2012. LPI Contribution No. 1667 (Abstract 6377).
Larson, H.P., Feierberg, M., Fink, U., Smith, H.A., 1979. Remote spectroscopic identification of carbonaceous chondrite mineralogies: Applications to Ceres and Pallas. Icarus 39, 257–271.
Lebofsky, L.A., 1978. Asteroid 1 Ceres: Evidence for water of hydration. Mon. Not. R. Astron. Soc. 182, 17–21.
Lebofsky, L.A., Feierberg, M.A., Tokunaga, A.T., Larson, H.P., Johnson, J.R., 1981. The 1.7- to 4.2-μm spectrum of asteroid 1 Ceres – Evidence for structural water in clay minerals. Icarus 48, 453–459.
Lebofsky, L.A. et al., 1985. Submillimeter observations of the asteroid 10 Hygiea. Icarus 63, 192–200.
Li, J.-Y. et al., 2006. Photometric analysis of asteroid 1 Ceres and surface mapping from HST observations. Icarus 182, 143–160.
Lippmann, F., 1973. Sedimentary Carbonate Minerals. Springer-Verlag, Berlin-Heidelberg, Federal Republic of Germany.
Lodders, K., 2003. Solar System abundances and condensation temperatures of the elements. Astrophys. J. 591, 1220–1247.
Lodders, K., Fegley Jr., B., 1998. The Planetary Scientist's Companion. Oxford University Press, New York.
Mackinnon, I.D.R., Buseck, P.R., 1979. High resolution transmission electron microscopy of two stony meteorites: Murchison and Kenna. Proc. Lunar Planet. Sci. Conf., 10, 937–949 (vol. 1).
Mackinnon, I.D.R., Zolensky, M.E., 1984. Proposed structures of poorly characterized phases in C2M carbonaceous chondrite matrices. Nature 309, 240–242.
Marchi, S. et al., 2013. High-velocity collisions from the lunar cataclysm recorded in asteroidal meteorites. Nat. Geosci. 6, 303–307.
Marion, G.M., Kargel, J.S., Catling, D.C., Lunine, J.I., 2012. Modeling ammonia–ammonium aqueous chemistries in the Solar System's icy bodies. Icarus 220, 932–946.
Markova, O.M., Yakovlev, O.I., Semenov, G.A., Belov, A.N., 1986. Some general results of experiments on evaporation of natural melts in the Knudsen cell. Geokhimiya 11, 1559–1569.
McCord, T.B., Sotin, C., 2005. Ceres: Evolution and current state. J. Geophys. Res. 110, E05009.
McCord, T.B., Castillo-Rogez, J., Rivkin, A., 2011. Ceres: Its origin, evolution and structure and Dawn's potential contribution. Space Sci. Rev. 163, 63–76.
McKinnon, W.B., 2008. Could Ceres be a refugee from the Kuiper belt? In: Asteroids, Comets, Meteors Conf. Abstract 8389.
McKinnon, W.B., 2012. Where did Ceres accrete? In: Asteroids, Comets, Meteors Conf. Abstract 6475.
Milliken, R.E., Rivkin, A.S., 2009. Brucite and carbonate assemblages from altered olivine-rich materials on Ceres. Nat. Geosci. 2, 258–261.
Mironenko, M.V., Melikhova, T.Yu., Zolotov, M.Yu., Akinfiev, N.N., 2008. GEOCHEQ_M: Program Complex for Thermodynamic and Kinetic Modeling of Geochemical Processes in Rock–Water–Gas Systems. Version 2008. Herald DGGGMS RAS. <http://www.scgis.ru/russian/cp1251/h_dgggms/1-2008/informbul-1_2008/mineral-22e.pdf>.
Mitchell, D.L. et al., 1996. Radar observations of asteroids 1 Ceres, 2 Pallas, and 4 Vesta. Icarus 124, 113–133.
Moody, J.B., 1976a. Serpentinization: A review. Lithos 9, 125–138.
Moody, J.B., 1976b. An experimental study on the serpentinization of iron-bearing olivines. Can. Mineral. 14, 462–478.
Moroz, L.V., Arnold, G., Korochantsev, A.V., Wasch, R., 1998. Natural solid bitumens as possible analogs for cometary and asteroid organics. Icarus 134, 253–268.
Mothé-Diniz, T., Di Martino, M., Bendjoya, P., Doressoundiram, A., Migliorini, F., 2001. Rotationally resolved spectra of 10 Hygiea and a spectroscopic study of the Hygiea family. Icarus 152, 117–126.
Mumpton, F.A., Thompson, C.S., 1966. The stability of brucite in the weathering zone of the New Idria serpentinites. Clays Clay Miner. 14, 249–257.
Mumpton, F.A., Thompson, C.S., 1975. Mineralogy and origin of the Coalinga asbestos deposit. Clays Clay Miner. 23, 131–144.
Navrotsky, A., Mazeina, L., Majzlan, J., 2008. Size-driven structural and thermodynamic complexity in iron oxides. Science 319, 1635–1638.
Niles, P.B., Zolotov, M.Yu., Leshin, L.A., 2009. Insights into the formation of Fe- and Mg-rich aqueous solutions on early Mars provided by the ALH 84001 carbonates. Earth Planet. Sci. Lett. 286, 122–130.
Pascale, F. et al., 2004. Vibrational spectrum of brucite, Mg(OH)(2): A periodic ab initio quantum mechanical calculation including OH anharmonicity. Chem. Phys. Lett. 396, 308–315.
Pizzarello, S., Williams, L.B., Lehmanc, J., Hollanda, G.P., Yargera, J.L., 2011. Abundant ammonia in primitive asteroids and the case for a possible exobiology. Proc. Natl. Acad. Sci. USA 108, 4303–4306.
Ragazzoni, R., Baruffolo, A., Marchetti, E., Ghedina, A., Farinato, J., Niero, T., 2000. Speckle interferometry measurements of the asteroids 10-Hygiea and 15-Eunomia. Astron. Astrophys. 354, 315–320.
Rivkin, A.S., Volquardsen, E.L., 2010. Rotationally-resolved spectra of Ceres in the 3-μm region. Icarus 206, 327–333.
Rivkin, A.S., Volquardsen, E.L., Clark, B.E., 2006. The surface composition of Ceres: Discovery of carbonates and iron-rich clays. Icarus 185, 563–567.
Rivkin, A.S. et al., 2011. The surface composition of Ceres. Space Sci. Rev. 101, 1–22.
Rosenberg, N.D., Browning, L., Bourcier, W.L., 2001. Modeling aqueous alteration of CM carbonaceous chondrites. Meteorit. Planet. Sci. 36, 239–244.
Rousselot, P. et al., 2011. A search for water vaporization on Ceres. Astron. J. 142, 125–131.
Rubin, A.E., Trigo-Rodríguez, J.M., Huber, H., Wasson, J.T., 2007. Progressive aqueous alteration of CM carbonaceous chondrites. Geochim. Cosmochim. Acta 71, 2361–2382.
Russell, C.T. et al., 2007. Dawn mission to Vesta and Ceres. Earth, Moon, Planets 101, 65–91.
Shock, E.L., Helgeson, H.C., Sverjensky, D.A., 1989. Calculation of the thermodynamic and transport properties of aqueous species at high pressures and temperatures: Standard partial and molar properties of inorganic neutral species. Geochim. Cosmochim. Acta 53, 2157–2183.
Shock, E.L., Sassani, D.C., Willis, M., Sverjensky, D.A., 1997. Inorganic species in geologic fluids: Correlations among standard molal thermodynamic properties of aqueous ions and hydroxide complexes. Geochim. Cosmochim. Acta 61, 907–950.
Takir, D., Emery, J.P., 2012. Outer main belt asteroids: Identification and distribution of four 3-μm spectral groups. Icarus 219, 641–654.
Thomas, P.C. et al., 2005. Differentiation of the asteroid Ceres as revealed by its shape. Nature 437, 224–226.
Tomeoka, K., Buseck, P., 1985. Indicators of aqueous alteration in CM carbonaceous chondrites: Microtextures of a layered mineral containing Fe, S, O, and Ni. Geochim. Cosmochim. Acta 49, 2149–2163.
Tornabene, L.L. et al., 2013. An impact origin for hydrated silicates on Mars: A synthesis. J. Geophys. Res.: Planets 118, 994–1012.
Travis, B.J., Schubert, G., 2005. Hydrothermal convection in carbonaceous chondrite parent bodies. Earth Planet. Sci. Lett. 240, 234–250.
Walsh, K.J., Morbidelli, A., Raymond, S.N., O'Brien, D.P., Mandell, A.M., 2011. A low mass for Mars from Jupiter's early gas-driven migration. Nature 475, 206–209.
Wasson, J.T., Rubin, A.E., 2010. Matrix and whole-rock fractionations in the Acfer 094 type 3.0 ungrouped carbonaceous chondrite. Meteorit. Planet. Sci. 45, 73–90.
Webster, W.J. et al., 1988. The microwave spectrum of asteroid Ceres. Astron. J. 95, 1263–1268.
Wilson, J.C., 2010. A new polymer model for estimating Gibbs free energy of formation (ΔG_F) of 7, 10 and 14 Å phyllosilicates at 25 °C and 1 bar. Clays in Natural & Engineered Barriers for Radioactive Waste Confinement, 4th Intl. Meeting (Abstract).
Wilson, L., Keil, K., Browning, L.B., Krot, A.N., Bourcier, W., 1999. Early aqueous alteration, explosive disruption, and reprocessing of asteroids. Meteorit. Planet. Sci. 34, 541–557.
Witteborn, F.C., Roush, T.L., Cohen, M., 2000. Thermal emission spectroscopy of 1 Ceres: Evidence for olivine. In: Sitko, M.L., Sprague, A.L., Lynch, D.K. (Eds.), Thermal Emission Spectroscopy and Analysis of Dust, Disks, and Regoliths, Astronom. Soc. of the Pacific Conf. Ser., vol. 196, pp. 197–203.
Wolery, T.J., Jove-Colon, C.F., 2004. Qualification of thermodynamic data for geochemical modeling of mineral–water interactions in dilute systems. Rep. ANL-WIS-GS-000003 REV 00, U.S. Dept. of Energy, Washington, DC.

Young, E.D., Zhang, K.K., Schubert, G., 2003. Conditions for pore water convection within carbonaceous chondrite parent bodies – Implications for planetesimal size and heat production. Earth Planet. Sci. Lett. 213, 249–259.
Zega, T.J., Buseck, P.R., 2003. Fine-grained rim mineralogy of the Cold Bokkeveld CM chondrite. Geochim. Cosmochim. Acta 67, 1711–1721.
Zolensky, M., McSween Jr., H.Y., 1988. Aqueous alteration. In: Kerridge, J.F., Matthews, M.S. (Eds.), Meteorites and the Early Solar System. University of Arizona Press, Tucson, pp. 114–143.
Zolensky, M.E., Bourcier, W.L., Gooding, J.L., 1989. Aqueous alteration on the hydrous asteroids: Results of EQ3/6 computer simulations. Icarus 78, 411–425.
Zolensky, M., Barret, R., Browning, L., 1993. Mineralogy and composition of matrix and chondrule rims in carbonaceous chondrites. Geochim. Cosmochim. Acta 57, 3123–3148.
Zolotov, M.Yu., 2009. On the composition and differentiation of Ceres. Icarus 204, 183–193.
Zolotov, M.Yu., 2012. Aqueous fluid composition in CI chondritic materials: Chemical equilibrium assessments in closed systems. Icarus 220, 713–729.
Zolotov, M.Y., Mironenko, M.V., 2007. Timing of acid weathering on Mars: A kinetic-thermodynamic assessment. J. Geophys. Res. 112, E07006.
Zolotov, M.Yu., Mironenko, M.V., Shock, E.L., 2006. Thermodynamic constraints on fayalite formation on parent bodies of chondrites. Meteorit. Planet. Sci. 41, 1775–1796.